Models for wind turbines - a collection

Baumgart, Andreas; Larsen, Gunner Chr.; Hansen, M.H.

Publication date:
2002

Document Version
Publisher's PDF, also known as Version of record

Risø-R-1352(EN)

Models for Wind Turbines – a Collection

Andreas Baumgart

Gunner C. Larsen, Morten H. Hansen (Eds.)

Risø National Laboratory, Roskilde, Denmark
February 2002

Abstract This report is a collection of notes which were intended to be short communications. Main target of the work presented is to supply new approaches to stability investigations of wind turbines. The author's opinion is that an efficient, systematic stability analysis can not be performed for large systems of differential equations (i.e. the order of the differential equations > 100), because numerical "effects" in the solution of the equations of motion as initial value problem, eigenvalue problem or whatsoever become predominant. It is therefore necessary to find models which are reduced to the elementary coordinates but which can still describe the physical processes under consideration with sufficiently good accuracy. Such models are presented.

ISBN 87–550–3083–1
ISBN 87–550–3085–8 (Internet)
ISSN 0106–2840

Print: Pitney Bowes Management Services Danmark A/S, 2002

Contents

1 Preface

During resent years, stability problems in wind turbine structures have obtained increasing attention due to the trend towards larger and more flexible structures. A well known example of a stability problem, that eventually might lead to failure of the whole structure or at least of vital parts of it, is the occurence of edgewise vibrations.

With this recognition, it become of interest to establish mathematical models that are able to describe such physical phenomenons and thereby also make it possible to identify such stability problems already in the design phase of a wind turbine structure.

As a follow up on this point of view, an initiative was taken in 1998 in the Aeroelastic group at Risø. The objective was to investigate feasible ways of modeling structural instabilities in wind turbine structures, and a post Doc. position was established with this purpose. The technical approach taken in the scientific work has been to follow the philosophy commonly used in aeroelastic modeling, and consequently select relative simple models for the structure as well as for the aerodynamics.

The study falls basically in three parts – one dealing with beam models, one dealing with an aerodynamic model expressed in terms of a few state variables, and finally the synthesis of these two elements into a stability analysis.

The aerodynamic loading (and damping) is intimately associated with the angle of attack of the incoming flow on the turbine blade – a fact that makes the structural coupling between blade flexture and torsion a matter of utmost importance. This is the background for the focus on a beam model including warping in the present study. In addition to the allowance of a kinematic coupling between flexture and torsion, the first torsional natural frequency turns out to be heavily affected by the inclusion of a warping degree of freedom which again has a strong impact on the occurence of flutter.

The possibility of obtaining suitable beam input parameters from an advanced FEM solution based on shell elements has also been investigated, and an algorithm computing these, based on output from ANSYS, has been established.

Damping is a central parameter in most stability analyses. For a wind turbine structure, the damping is composed of structural damping and aerodynamic damping. In contrast to the simply and widely used Rayleigh structural damping formulation, some materials exhibit a damping behaviour that in addition to the strain velocity also depends on the strain frequency. Such a damping material model expressed in inner variables has been reviewed. The aerodynamic damping inherent in wind turbine modeling directly results from the aerodynamic model.

A simple aerodynamic model founded on two independent physical processes – the generation of pressure waves from a vibrating profile and flow circulation/detachment related to a given profile – has been formulated in terms of a few state variables (5). This aerodynamic model has, together with the formulated beam model, subsequently been used to perform a number of stability studies.

The stability studies are all based on linear stability analysis (i.e. small pertubations from a given equilibrium situation), and range in complexity from a single airfoil cross section element, with only one deflectional degree of freedom, ex-

posed to aerodynamic forces to a full elastic wind turbine blade rotating around a spatially fixed axis and exposed to the relevant aerodynamic forces.

Gunner C. Larsen
Morten H. Hansen

2 Author's Notes

This report is a collection of notes which were intended to be short communications. It documents the author's work over a period of two years for the program area Aeroelastic Design in the department of Wind Energy Deparment, Risø. It was initiated on the occasion that the author resigns from his work with Risø.

Due to the "stand alone" nature of the individual notes, repetition of arguments and ideas could not be avoided. The order of the notes does not necessarily correspond to a chronological order of the author's work but is chosen to document an evolution of ideas.

Main target of the work was to supply new approaches to stability investigations of wind turbines. Since the work was not directly related to a concrete project, the ideas were meant to "diffuse" into the ongoing work by intense discussion and the elaboration of "stripped" models (i.e. computer programs) showing the capabilities and feasibility of the approach.

The author's opinion is that an efficient, systematic stability analysis can not be performed for large systems of differential equations (i.e. the order of the differential equations > 100), because numerical "effects" in the solution of the equations of motion as initial value problem, eigenvalue problem or whatsoever become predominant. It is necessary to find models which are reduced to the elementary coordinates but which can still describe the physical processes under consideration with sufficiently good accuracy.

A wind turbine model consists of a sub-model for the turbine structure itself, a flow field sub-model which describes the overall flow of air in the vicinity of the turbine and of an interface sub-model that connects flow and structure.

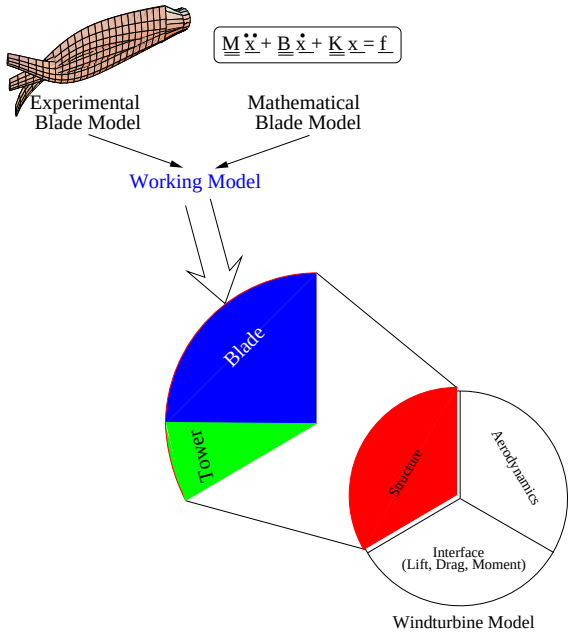

Figure 1: Structure–, aerodynamics– and interface-models with the structure-branch shown exploded.

Depending on the physical mechanisms under consideration, the model-components have to be elaborated (or chosen) appropriately.

The author is an engineer with a background in structural mechanics.

3 Theory of Rods applied to Wind Turbine Blades

3.1 Introduction

The modelling of wind turbine blades presents a difficult challenge. Their complicated geometry and material composition – as presented for example by a change of the cross sections shape along the length and the use of fiber materials – causes an elastic coupling of the blades flexure, torsion, extension and shear. For aeroelastic computations of wind loads and dynamic stability analysis of a wind turbines motion, this coupling mechanism is of vital interest.

Finite Element (FE) methods give a detailed description of deformations of a loaded blade, but their large number of degrees of freedom and the high eigenfrequencies of such a model associated with a required fine spatial discretization cause extremely long computation times when simulating in the time domain.

One alternative to FE models is the development of a blade model relying on the theory of rods. The basic idea is to characterize the blade motion by few (say 10) partial differential equations in which there is but one independent spatial variable. These partial differential equations can easily be further discretized to ordinary differential equations as desired when simulating in the time domain.

In the following, we shall derive such models, employing the principle of virtual work. The main focus will be on the virtual work of elastic stresses. For simplicity, we investigate a cantilevered blade on a fictitious test stand. The computation of virtual works of d'Alembert forces for a blade, which is attached to an operating turbine, is then straight forward. Of major importance is also damping associated with deformations of the blade. This problem is naturally very closely related to the computation of virtual work of elastic stresses, but will not be discussed here.

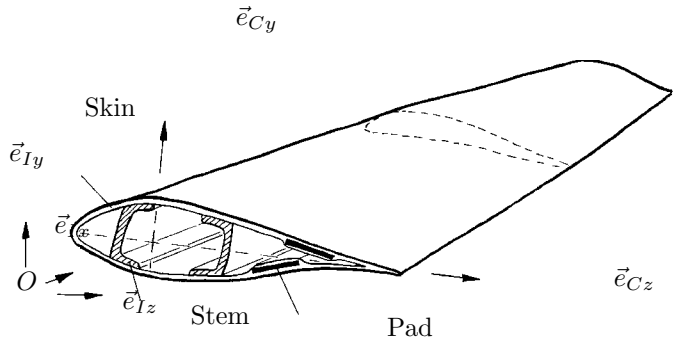

Figure 2: Coordinate systems $\underline{\vec{e}}_I$ and $\underline{\vec{e}}_C$ of the blade.

Procedure and Notation

We derive a linear system of partial differential equations governing small deformations of a wind turbine blade. A real blade – as depicted in Figure 2 – is often made from a closed, shell-like skin, which forms the airfoil and a stiffening stem in the inside. Pads made from foam-materials thicken the skin in order to increase the local bending stiffness. The blade material is supposed to be linear elastic and piecewise isotropic. In the description of the blade kinematics, we follow [2]; in

the formulation of the virtual work of elastic stresses, we rely on [14]. A computer algebra program (Mathematica) is used to perform cumbersome analytical and numerical computations. For a simple test case, eigenfrequencies and eigenmodes of the blade are computed.

The following notations are used :

A vector $\vec{r}$ is represented by

$$\vec{r} = \underline{r}\ \underline{\vec{e}}\ ,$$

where $\underline{r} = \{r_x, r_y, r_z\}^T$ is the coordinate triple with components r_i, $i = \{x, y, z\}$ of $\vec{r}$ in the coordinate system $\underline{\vec{e}} = \{\vec{e}_x, \vec{e}_y, \vec{e}_z\}^T$, spanned by the orthogonal unit vectors $\vec{e}_i$, $i = \{x, y, z\}$. Thus $\vec{(.)}$ denotes a vector, $\underline{(.)}$ a column matrix. We transform between coordinate systems $\underline{\vec{e}}$ and $\underline{\vec{e}}^{\,*}$ using the transformation matrices

$$\underline{\underline{D}}_x(\varphi_x) = \begin{bmatrix} 1 & 0 & 0 \\ 0 & \cos(\varphi_x) & \sin(\varphi_x) \\ 0 & -\sin(\varphi_x) & \cos(\varphi_x) \end{bmatrix} \quad ,$$

$$\underline{\underline{D}}_y(\varphi_y) = \begin{bmatrix} \cos(\varphi_y) & 0 & -\sin(\varphi_y) \\ 0 & 1 & 0 \\ \sin(\varphi_y) & 0 & \cos(\varphi_y) \end{bmatrix} \quad \text{and}$$

$$\underline{\underline{D}}_z(\varphi_z) = \begin{bmatrix} \cos(\varphi_z) & \sin(\varphi_z) & 0 \\ -\sin(\varphi_z) & \cos(\varphi_z) & 0 \\ 0 & 0 & 1 \end{bmatrix} \quad .$$

The $\underline{\underline{D}}_i$ rotate $\underline{\vec{e}}$ into the new coordinate system $\underline{\vec{e}}^{\,*}$ by a rotation φ_i around the i-axis:

$$\underline{\vec{e}}^{\,*} = \underline{\underline{D}}_i(\varphi_i)\ \underline{\vec{e}}\ .$$

3.2 Reference Configuration

The blade is clamped horizontally at its root in a fictitious rigid test stand.

An inertial cartesian coordinate system $\underline{\vec{e}}_I = \{\vec{e}_{Ix}, \vec{e}_{Iy}, \vec{e}_{Iz}\}^T$ with coordinates x, y, z has its origin O at the blade root. The coordinate system $\underline{\vec{e}}_I$ is aligned, so that $\vec{e}_{Ix}$ is horizontally and points in the blades longitudinal direction (see Figure 2). A cross section x^* of the blade is defined to consist of all material particles, which have in the strainless reference configuration the x-coordinate x^*. For convenience, $\vec{e}_{Ix}$ should be layed near the curve, which connects the mass centers of all cross sections x. $\vec{e}_{Iy}$ and $\vec{e}_{Iz}$ are chosen conveniently.

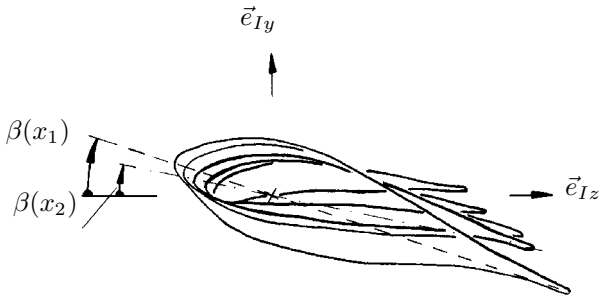

Figure 3: Twist of the blade in its reference configuration as seen from the blade root ($x_2 > x_1$).

Let $\beta(x)$ be the angle between the cord of a blades cross section x and $\vec{e}_{Iz}$ (see Figures 3 and 2) so that a new coordinate system $\underline{\vec{e}}_C$ is defined by

$$\underline{\vec{e}}_C = \underline{\underline{D}}_x(\beta(x))\ \underline{\vec{e}}_I \tag{1}$$

with $\{x, y_C, z_C\}^T\ \underline{\vec{e}}_C = \{x, y, z\}^T\ \underline{\vec{e}}_I$.

The local vector $\vec{r}_{P,ref}$ from O to any material point P of the blade in its reference configuration is

$$\vec{r}_{P,ref} = \{x, 0, 0\}^T \underline{\vec{e}}_I + \{0, y_C, z_C\}^T \underline{\vec{e}}_C\ .$$

Next we define the geometry of the blade. For simplicity, we define the outer surface of the blade by low order polynomials in a new coordinate s, $s \in [0, 1]$. Let the blades surface vector be

$$\vec{r}_S(s, x) = \{x, \hat{y}_C(s, x), \hat{z}_C(s, x)\}\ \underline{\vec{e}}_C\ , \tag{2}$$

with

$$\begin{aligned} \hat{y}_S(s, x) &= \ell_S(x) \cdot y_0 6\sqrt{3} s \left(1 - 3s + 2s^2\right) \text{ and} \\ \hat{z}_S(s, x) &= \ell_S(x) \cdot \left(4\left(s - \frac{1}{2}\right)^2 - \frac{1}{4}\right)\ , \end{aligned} \tag{3}$$

where $\ell_S(x)$ is a scaling length and y_0 the thickness to chord length ratio of the blades cross section (see Figure 4).

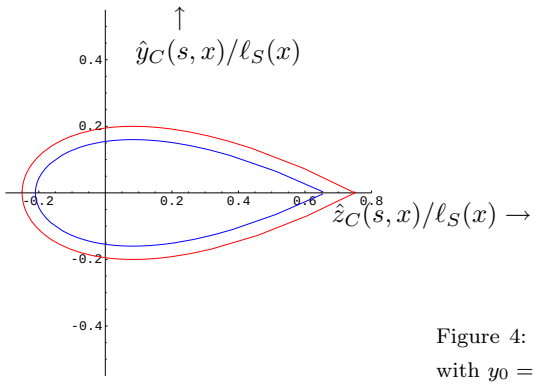

Figure 4: Blade cross section with $y_0 = 0.2$.

A unit vector tangential to the blades surface is

$$\vec{r}_S^{\,t}(s, x) = \frac{\dfrac{\partial \vec{r}_S(s, x)}{\partial s}}{\left|\dfrac{\partial \vec{r}_S(s, x)}{\partial s}\right|}\ ,$$

and the unit vector perpendicular to $\vec{r}_S^{\,t}(s,x)$ and $\vec{e}_{Cx}$ be

$$\vec{r}_S^{\,n}(s,x) = \vec{r}_S^{\,t}(s,x) \times \vec{e}_{Ix} \ .$$

Any material point of the blade can now be identified as

$$\vec{r}_{P,ref}(x,s,h) = \vec{r}_S(s,x) - h\ \vec{r}_S^{\,n}(s,x)\ , h \in [0,H]\ , \tag{4}$$

where H is the thickness of the blades skin (see Figure 5).

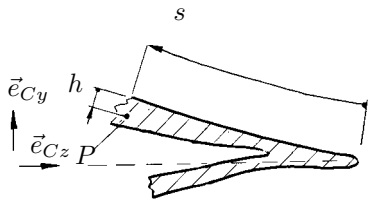

Figure 5: Spatial Coordinates s and h.

In the following, no stem as drawn in Figure 2 will be accounted for.

The form of the equations of motion is unaffected by assuming a simple blade geometry as described above. The considerations presented in the following are valid for arbitrary cross sections and arbitrary, but piecewise homogeneous and isotropic, materials. No principal problems will arise, when more complicated geometries are considered.

3.3 Kinematics

Let the position of a material point P of the blade in its deformed configuration be

$$\begin{aligned} \vec{r}_P(x,y,z,t) = \quad & \{x + u_x(x,t), u_y(x,t), u_z(x,t)\}^T \underline{\vec{e}}_I + \\ & \left\{ \sum_{i=1}^{3} \psi_i(x,t) \cdot w_i(y_C, z_C), y_C, z_C \right\} \\ & \times \underline{\underline{D}}_z(\varphi_z(x,t)) \underline{\underline{D}}_y(\varphi_y(x,t)) \underline{\underline{D}}_x(\varphi_x(x,t))\ \underline{\vec{e}}_C\ , \end{aligned} \tag{5}$$

where $u_x(x,t)$, $u_y(x,t)$, $u_z(x,t)$, $\varphi_x(x,t)$, $\varphi_y(x,t)$, $\varphi_z(x,t)$, $\psi_1(x,t)$, $\psi_2(x,t)$ and $\psi_3(x,t)$ are dependent variables of the blades motion and the $w_i(y_C, z_C)$ are warping form-functions for cross section x. We define

$$w_1 = y_C z_C\ , w_2 = y_C^2 \text{ and } w_3 = z_C^2$$

and linearize (5) with respect to all dependent variables:

$$\begin{aligned} \vec{r}_P(x,y,z,t) = \ & (u_x(x,t) + \ \varphi_y(x,t) \cdot (z\cos(\beta(x)) + y\sin(\beta(x))) - \\ & \varphi_z(x,t) \cdot (y\cos(\beta(x)) - z\sin(\beta(x))) + \\ & \psi_1(x,t) \cdot (z\cos(\beta(x)) + y\sin(\beta(x))) \\ & \cdot (y\cos(\beta(x)) - z\sin(\beta(x))) + \\ & \psi_2(x,t) \cdot (y\cos(\beta(x)) - z\sin(\beta(x)))^2 + \\ & \psi_3(x,t) \cdot (z\cos(\beta(x)) + y\sin(\beta(x)))^2) \cdot \vec{e}_{Ix} \\ & (u_y(x,t) - \varphi_x(x,t)(z\cos(2\beta(x)) + y\sin(2\beta(x)))) \cdot \vec{e}_{Iy} + \\ & (u_z(x,t) + \varphi_x(x,t)(y\cos(2\beta(x)) - z\sin(2\beta(x)))) \cdot \vec{e}_{Iz}\ . \end{aligned} \tag{6}$$

We denote $\vec{r}_P(x,0,0,t) =: \vec{r}_R(x,t)$ reference curve R of the blade. Let the column matrix of dependent variables be

$$\underline{q}(x,t) := \{u_x(x,t), u_y(x,t), u_z(x,t), \varphi_x(x,t), \varphi_y(x,t), \varphi_z(x,t), \psi_1(x,t), \psi_2(x,t), \psi_3(x,t)\}^T \ .$$

For $\psi_i \equiv 0$, $i = \{1,2,3\}$, the motions of the blades cross section x are translations $u_x(x,t)$, $u_y(x,t)$ and $u_z(x,t)$ describing the position of R and rotations $\varphi_x(x,t)$, $\varphi_y(x,t)$ and $\varphi_z(x,t)$ of the cross section about R. Then, a cross section would remain plane after deformation. The resulting equations of motion would be the same as in Timoshenko's theory for beams. Further restrictions, as

$$\begin{aligned} \varphi_y &= -\cos(\beta(x))\frac{\partial u_z}{\partial x} - \sin(\beta(x))\frac{\partial u_y}{\partial x} \text{ and} \\ \varphi_z &= \cos(\beta(x))\frac{\partial u_y}{\partial x} - \sin(\beta(x))\frac{\partial u_z}{\partial x} \end{aligned} \tag{7}$$

would eventually lead to the equations of motion for an Euler Bernoulli Beam.

The functions ψ_i allow for warping of a cross section. In the x-component r_{Px} of $\vec{r}_P(x,y,z,t)$ in (6), the dependent variables u_x, φ_y, φ_z, ψ_1, ψ_2 and ψ_3 can be seen as the coefficients of a second order Taylor series in y_C and z_C for the displacements of the particles of cross section x:

$$\begin{aligned} r_{Px} - r_{P,ref\ x} = \quad & 1 \cdot u_x(x,t) \\ - \quad & y_C \cdot \varphi_z(x,t) \\ + \quad & z_C \cdot \varphi_y(x,t) \\ + \quad & y_C z_C \cdot \psi_1(x,t) \\ + \quad & y_C^2 \cdot \psi_2(x,t) \\ + \quad & z_C^2 \cdot \psi_3(x,t) \ . \end{aligned}$$

3.4 Equations of Motion

The equations of motion are derived using the principle of virtual work in conjunction with Galerkin's method. The principle of virtual work is taken as

$$\begin{aligned} \delta W &= \delta W_V + \delta W_E + \delta W_F \\ &\stackrel{!}{=} 0 \ , \end{aligned} \tag{8}$$

where δW_V is the virtual work of gravity and d'Alembert (inertia) volume forces, δW_E is the virtual work of the blades internal stresses due to deformations and δW_F is the virtual work of external forces.

For convenience, we shall from now on use the following abbreviations :

$$\begin{aligned} (.)' &:= \frac{\partial}{\partial x}(.);, \\ \dot{(.)} &:= \frac{\partial}{\partial t}(.);. \end{aligned}$$

Internal Stresses

We do not account for material damping, so we may write the relation between stresses σ_{ij} and strains ε_{ij} using Hook's law

$$\begin{aligned}\sigma_{ij} &= 2\mu\varepsilon_{ij} + \lambda\varepsilon_{kk}\cdot\delta_{ij} \\ &= \sigma_{ji} \qquad\qquad i,j,k \in \{x,y,z\}\ ,\end{aligned} \tag{9}$$

with Lamé's constants μ, λ and the Kronecker symbol δ_{ij}. Lamé's constants are related to the modulus of elasticity E, the shear modulus G and Poisson's ratio ν by

$$\begin{aligned}\mu &= G \\ &= \frac{E}{2(1+\nu)}\end{aligned} \quad \text{and} \quad \lambda \;=\; \nu\frac{E}{(1+\nu)(1-2\nu)}\ .$$

We may neglect the virtual work of σ_{yy} and σ_{zz} due to the slenderness of the blade, so (9) yields

$$\begin{aligned}\sigma_{xx} &= \frac{\mu(3\lambda+2\mu)\varepsilon_{xx}}{\lambda+\mu}\ , \\ \sigma_{xy} &= 2\mu\varepsilon_{xy}\ , \\ \sigma_{xz} &= 2\mu\varepsilon_{xz}\ , \\ \sigma_{yz} &= 2\mu\varepsilon_{yz}\ , \\ \varepsilon_{yy} &= -\frac{\lambda\varepsilon_{xx}}{2(\lambda+\mu)} \text{ and} \\ \varepsilon_{zz} &= -\frac{\lambda\varepsilon_{xx}}{2(\lambda+\mu)}\ .\end{aligned} \tag{10}$$

The strains ε_{ij} are functions of the blade coordinates $\underline{q}(x,t)$. Greens strain tensor states

$$\begin{aligned}\varepsilon_{xx} &= \frac{\partial r_x}{\partial x}\ , \\ \varepsilon_{yy} &= \frac{\partial r_y}{\partial y}\ , \\ \varepsilon_{zz} &= \frac{\partial r_z}{\partial z}\ , \\ \varepsilon_{yz} &= \frac{1}{2}\left(\frac{\partial r_z}{\partial y}+\frac{\partial r_y}{\partial z}\right) &&= \varepsilon_{zy}\ , \\ \varepsilon_{zx} &= \frac{1}{2}\left(\frac{\partial r_x}{\partial z}+\frac{\partial r_z}{\partial x}\right) &&= \varepsilon_{xz}\ , \\ \varepsilon_{xy} &= \frac{1}{2}\left(\frac{\partial r_y}{\partial x}+\frac{\partial r_x}{\partial y}\right) &&= \varepsilon_{yx}\end{aligned} \tag{11}$$

(see Washizu ([14], 1982), p.83). With the blade volume V, the virtual work of internal stresses can now be computed as:

$$\delta W_E := -\int_V \sigma_{ij}\cdot\delta\varepsilon_{ij}\mathrm{d}V\ ,\ i,j\in\{x,y,z\}\ .$$

Volume Forces

Volume forces on the blade are d'Alemberts inertia forces and gravity forces. With the material density ϱ, the variation of the local vector $\delta\vec{r}_P$ and the vector of gravity $\vec{g}_E$ we calculate the virtual work of these forces to be

$$\delta W_V := \int_V \varrho \cdot \left(-\ddot{\vec{r}}_P + \vec{g}_E \right) \delta\vec{r}_P \, \mathrm{d}V \; . \tag{12}$$

In the following, we do not account for terms resulting from $\vec{g}_E$.

External Forces

Let $\vec{f}(x,t)$ be a prescribed external force per unit blade length, which acts on R and $\vec{m}(x,t) = m_x(x,t)\ \vec{e}_{Ix}$ be an external moment per unit blade length around the x-axis. Then

$$\delta W_E := -\int_\ell \left(\vec{f}\,\delta\vec{r}_R \ + \ m_x\,\delta\varphi_x \right) \mathrm{d}x \; . \tag{13}$$

Form-functions in x

Equation (5) defines displacements of material points of a blades cross section x in the coordinates $\underline{q}(x,t)$.

We obtain the weak form of the partial differential equations for $\underline{q}$ by performing the integration over cross section x in (8) and we could – by partial differentiation – obtain the differential equations and the so called mechanical boundary conditions for all $\underline{q}(x,t)$. However, we seek ordinary differential equations for the blades motion, so we discretize further.

We choose few, low order polynomials as form-functions in x. They must fulfill all geometric boundary conditions, corresponding to a (clamped) cantilevered beam

$$\begin{aligned} u_x(0,t) &= 0 \; , \\ u_y(0,t) &= 0 \; , \\ u_z(0,t) &= 0 \; , \\ \varphi_x(0,t) &= 0 \; , \\ \varphi_y(0,t) &= 0 \quad \text{and} \\ \varphi_z(0,t) &= 0 \; . \end{aligned} \tag{14}$$

Let

$$
\begin{aligned}
u_x(x,t) &= U_x(t)\left(\frac{x}{\ell}\right) , \\
u_y(x,t) &= U_y(t)\left(\frac{x}{\ell}\right)^2 , \\
u_z(x,t) &= U_z(t)\left(\frac{x}{\ell}\right)^2 , \\
\varphi_x(x,t) &= \Phi_x(t)\left(\frac{x}{\ell}\right) , \\
\varphi_y(x,t) &= \Phi_y(t)\left(\frac{x}{\ell}\right) , \\
\varphi_z(x,t) &= \Phi_z(t)\left(\frac{x}{\ell}\right) , \\
\psi_1(x,t) &= \Psi_{1,0}(t)\,(1-\frac{x}{\ell}) + \Psi_{1,1}(t)\,\left(\frac{x}{\ell}\right) , \\
\psi_2(x,t) &= \Psi_{2,0}(t)\,(1-\frac{x}{\ell}) + \Psi_{2,1}(t)\,\left(\frac{x}{\ell}\right) , \\
\psi_3(x,t) &= \Psi_{3,0}(t)\,(1-\frac{x}{\ell}) + \Psi_{3,1}(t)\,\left(\frac{x}{\ell}\right)
\end{aligned}
\tag{15}
$$

be an appropriate discretization of the blades motion and let

$$
\underline{Q}(t) = \{U_x(t), U_y(t), U_z(t), \Phi_x(t), \Phi_y(t), \Phi_z(t), \Psi_{1,0}(t), \Psi_{1,1}(t), \Psi_{2,0}(t), \Psi_{2,1}(t), \Psi_{3,0}(t), \Psi_{3,1}(t)\}^T .
$$

From (8), we thus obtain a system of linear, ordinary differential equations

$$
\underline{\underline{M}}\,\ddot{\underline{Q}}(t) + \underline{\underline{K}}\,\underline{Q}(t) = \underline{F}(t) . \tag{16}
$$

Integration in (8) over the blade volume V involves a long sum of complicated integrals, which are mainly due to the pretwist $\beta(x) := \beta(\ell)x/\ell$ of the blade. These integrals are solved numerically. Note that in the integration over V the infinitesimal volume $\mathrm{d}x\,\mathrm{d}y\,\mathrm{d}z$ is conveniently expressed as a function of $\mathrm{d}x$, $\mathrm{d}s$ and $\mathrm{d}h$.

Reduction of the Number of State Variables

Usually, the motions described by $u_x(x,t)$, $u_y(x,t)$, $u_z(x,t)$, $\varphi_x(x,t)$, $\varphi_y(x,t)$, $\varphi_z(x,t)$, $\psi_1(x,t)$, $\psi_2(x,t)$ and $\psi_3(x,t)$ have very different characteristic time scales. Let us assume, that the flexural deflections $u_y(x,t)$, $u_z(x,t)$ and the rotation $\varphi_x(x,t)$ are motions of the blade, which dominate the "slow" blade motion, and that the other coordinates dominate "fast" blade motions. We call a motion "slow", when its oscillation frequency lies below a critical predefined frequency ω_{crit}. The magnitude of ω_{crit} is directly related to the characteristic time scale of the physical process, which shall be modelled (for example flutter or whirl). Thus, a motion is "fast", if its oscillation frequency lies well above ω_{crit}. We shall now describe, how the state variables associated with fast motions can be eliminated.

We consider an imaginary experiment where we slowly deflect the blade in u_y, u_z and φ_x from rest. This deflection invokes fast oscillations in the other coordinates, which will – due to the material damping in real materials – decay rapidly. Thus, the motions in u_x, φ_y, φ_z, ψ_1, ψ_2 and ψ_3 are slaved to the motions in u_y, u_z and φ_x. The motions in these coordinates can be regarded as quasistatic and we take this as the justification for the negligence of the d'Alembert forces associated with these coordinates. The new linear equations are then written with

$$
\underline{Z}(t) = \left\{\ddot{U}_y(t), \ddot{U}_z(t), \ddot{\Phi}_x(t), U_x(t), \Phi_y(t), \Phi_z(t), \Psi_{1,0}(t), \Psi_{1,1}(t), \Psi_{2,0}(t), \Psi_{2,1}(t), \Psi_{3,0}(t), \Psi_{3,1}(t)\right\}^T
$$

and for $\delta W_F \equiv 0$ as

$$\underline{\underline{A}}\,\underline{Z} + \underline{\underline{B}} \begin{pmatrix} U_y \\ U_Z \\ \Phi_x \end{pmatrix} = \underline{0}\,, \tag{17}$$

where $\underline{\underline{A}}$ is a 12×12 matrix and $\underline{\underline{B}}$ a 12×3 matrix.

3.5 Eigenvalues and Eigenvectors

Equation (17) defines an eigenvalue problem in U_y, U_z and Φ_x which we solve for the parameters specified in Section 3.7.

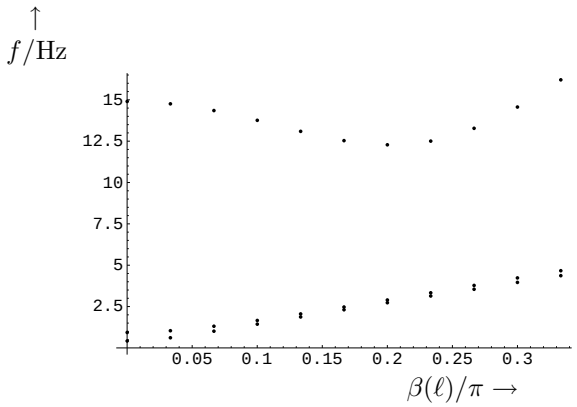

Figure 6: Eigenfrequencies of the blade as function of the blades pretwist $\beta(\ell)$.

In Figure 6, the eigenfrequencies of the blade for different pretwists $\beta(x)$ are given. The highest eigenfrequencies are always dominated by torsional vibrations, the two other eigenfrequencies belong to mainly flexural vibrations.

In Figures 7, 8 and 9, the motion of the blade at $x = \ell$ is sketched. Depicted are the positions of a massless rod, which is rigidly attached to the blades end, and which is perpendicular to the x-axis and parallel to the y-axis when the blade is in its reference configuration.

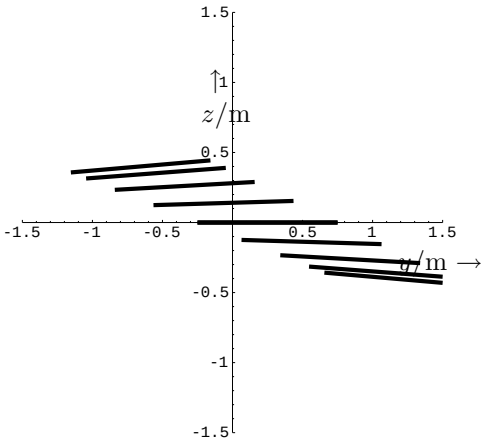

Figure 7: Images of a rod, which is rigidly connected to the blade at $x = \ell$ as the blade swings in its 1^{st} eigenmode ($\omega = 14.49\ 1/s$). The blade is pretwisted with $\beta(\ell) = \pi/6$.

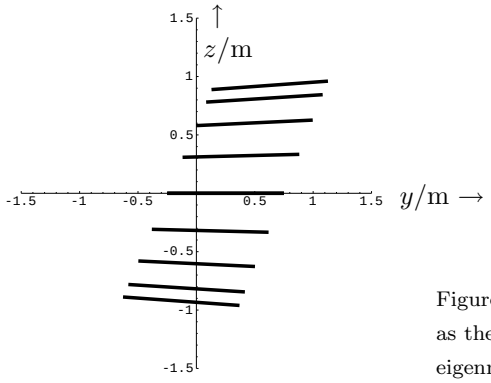

Figure 8: Images of the rod as the blade swings in its 2^{nd} eigenmode ($\omega = 15.50\ 1/s$).

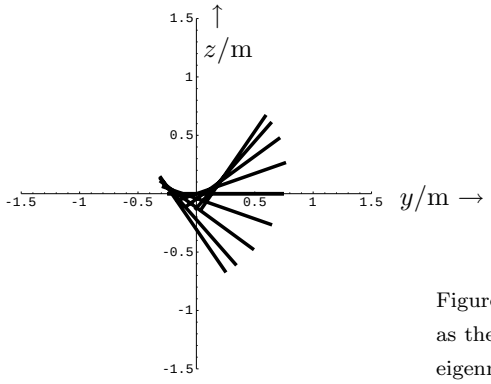

Figure 9: Images of the rod as the blade swings in its 3^{rd} eigenmode ($\omega = 78.74\ 1/s$).

In Section 3.7, the numerical values for eigenfrequencies and eigenvectors are given.

The elastic coupling between the individual coordinates as a function of the pretwist can best be seen in the following figures. A load $F_z \cdot \vec{e}_{Iz}$ is applied to the blade at $x = \ell$, thus $\vec{f} = \bar{\delta}(x - \ell)\ F_z\ \vec{e}_{Iz}$ using the Dirac fuction $\bar{\delta}$ (see (13)). F_z is chosen, so that $U_Z \equiv 1$ m holds (see Figure 11).

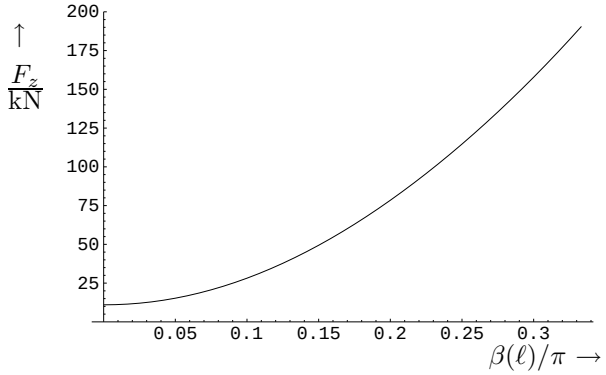

Figure 10: Applied force F_z as function of the blades pretwist $\beta(\ell)$. F_z is chosen, so that $U_Z \equiv 1$m.

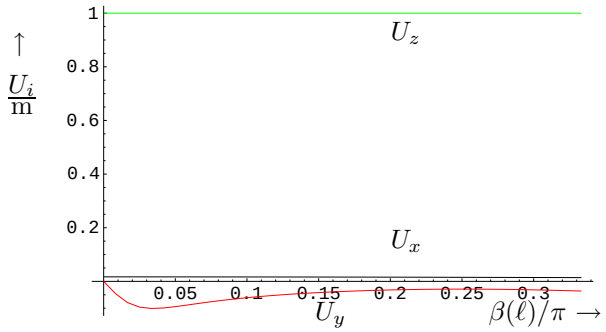

Figure 11: Coordinates U_x, U_y and U_z.

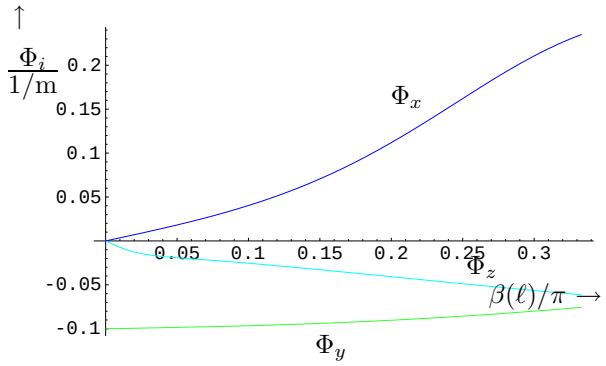

Figure 12: Coordinates Φ_x, Φ_y and Φ_z.

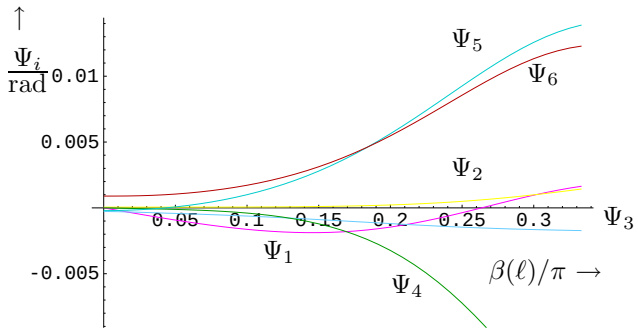

Figure 13: Coordinates Ψ_1, Ψ_2, Ψ_3, Ψ_4, Ψ_5 and Ψ_6.

3.6 Conclusion

The blade model accounts for an elastic coupling of the blades flexure, torsion, extension and shear. Its dependent coordinates describe translation and rotation as well as warping of the blades cross section. Using the principle of virtual work, the weak formulation for ten linear partial differential equations in the longitudinal spatial coordinate x and time t was derived. These equations of motion were discretized with respect to x and the number of degrees of freedom was further reduced to three, employing the concept of "slow" and "fast" motions. Numerical results show the dependence of eigenfrequencies from the blades pretwist and eigenmodes of the blade for $\beta(\ell) = \pi/6$.

The most important aspect of the model is the elastic coupling of flexure and torsion.

In the low frequency range, such as the bending of an operating blade under gravitational loads, the momentum of the blade around its longitudinal axis oscillates with the rotational speed of the rotor and might thus induce a whirling motion of the rotor axis.

For high frequency ranges, this coupling will be most important for the onset of flutter oscillations, depending on weather an increasing lateral airload increases or decreases the blades pitch and the respective aerodynamic load.

For stability analysis of wind turbines, this coupling might be essential.

A major model uncertainty arises from the chosen discretization of the blade. While assumed functions as in u_x, u_y, u_z, φ_x, φ_y and φ_z are well established and simplifications as in (7) might even be tolerable for a blade, no such experience exists for the warping of a pretwisted blade. For the discretization of the blade with respect to x, the same applies. These uncertainties could be solved employing a commercial FE program.

An appropriate model for material damping of the blade presents another problem. The Rayleigh damping-model (damping forces are proportional to the deformation velocity) is for plastics only valid in the low frequency range, say up to 20 Hz. Better models for material damping are given for example in [1].

But even the introduction of the simple Rayleigh damping model into (9) would produce first order time derivatives with respect to all coordinates and thus prohibit a reduction of the degrees of freedom as in Subsection 3.4.

3.7 Appendix

Eigensolutions

pretwist $\beta(\ell)/\pi$	eigenvalues $\omega_1/(1/\mathrm{s})$ $\omega_2/(1/\mathrm{s})$ $\omega_3/(1/\mathrm{s})$	eigenvectors $\{\hat{U}_{y1}/\mathrm{m},\hat{U}_{z1}/\mathrm{m},\hat{\Phi}_{x1}/\mathrm{rad}\}$ $\{\hat{U}_{y2}/\mathrm{m},\hat{U}_{z2}/\mathrm{m},\hat{\Phi}_{x2}/\mathrm{rad}\}$ $\{\hat{U}_{y3}/\mathrm{m},\hat{U}_{z3}/\mathrm{m},\hat{\Phi}_{x3}/\mathrm{rad}\}$
0	2.61	$-16\{1.,-5.5510,\ -0.00116\}$
	5.85	$\{0.426,\ \ 0.905,-0.000497\}$
	93.6	$-17\{0.183,\ 5.7710,\ \ \ 0.983\}$
1/30	3.89	$\{0.999,-0.0515,-0.00288\}$
	6.53	$\{0.0535,\ \ 0.998,\ \ 0.0116\}$
	92.7	$\{0.183,\ 0.0127,\ \ \ 0.983\}$
1/15	6.33	$\{0.994,-0.107,-0.00878\}$
	8.21	$\{0.111,\ 0.993,\ \ 0.0248\}$
	90.2	$\{0.181, 0.0251,\ \ \ 0.983\}$
1/10	9.02	$\{0.984,-0.175,-0.0214\}$
	10.4	$\{0.18,\ 0.983,\ 0.0408\}$
	86.4	$\{0.179, 0.0369,\ \ 0.983\}$
2/15	11.8	$\{0.963,-0.266,-0.0457\}$
	12.9	$\{0.27,\ 0.961,\ 0.0588\}$
	82.3	$\{0.177, 0.0477,\ \ 0.983\}$
1/6	14.5	$\{0.919,-0.385,-0.0875\}$
	15.5	$\{0.385,\ \ 0.92,\ 0.0735\}$
	78.7	$\{0.174, 0.0573,\ \ 0.983\}$
1/5	17.1	$\{0.85,-0.506,-0.144\}$
	18.2	$\{0.499,\ 0.864,\ 0.076\}$
	77.1	$\{0.172, 0.0661,\ 0.983\}$
7/30	19.7	$\{0.787,-0.583,\ -0.2\}$
	21.	$\{0.572,\ 0.818,0.0651\}$
	78.5	$\{0.169, 0.0749,\ 0.983\}$
4/15	22.3	$\{0.754,-0.612,-0.237\}$
	23.8	$\{0.599,\ 0.799, 0.0481\}$
	83.4	$\{0.165, 0.0847,\ 0.983\}$
3/10	24.9	$\{0.748,-0.613,-0.255\}$
	26.6	$\{0.598,\ 0.801, 0.0311\}$
	91.5	$\{0.159, 0.0954,\ 0.983\}$
1/3	27.4	$\{0.757, -0.6,-0.261\}$
	29.3	$\{0.583,0.812, 0.0165\}$
	102.	$\{0.151,0.106,\ 0.983\}$

Parameter

parameter	value
ℓ	20 m
H	2 cm
E	$2 \cdot 10^{10}$ N/m^2
ν	0.3
ϱ	8000 kg/m^3
$\beta(x)$	$\beta(\ell)\frac{x}{\ell}$
$\ell_S(x)$	$\left(1 - \frac{x}{2\ell}\right)$ m

4 A Mathematical Model for Wind Turbine Blades – including a comparison of model and experiments

A mathematical model for an elastic wind turbine blade mounted on a rigid test stand is derived and compared with experimental results. The linear equations of motion describe small rotations of the test stand as well as blade lateral deflections and rotation of the cord.
Warping, extension and tilt of the cross sections are slaved to the afore mentioned dependent coordinates in order to reduce the number of state variables.
Using the principle of virtual work, a procedure is employed which combines the volume discretization of general 3D-FEM with the approach of global form functions (stretching over the whole blade length).
The equations of motion are solved as an eigenvalue problem and results are compared with an experimental modal analysis of a 19 m long blade. The computed eigenfrequencies fit well, but the model under-estimates the blades cord rotation. Parameter studies show the effect of warping. Despite of the few degrees of freedom and uncertainties in model parameters, the mathematical model approximates the measured blade dynamics well.

4.1 Equations of Motion

We develop a mathematical model for a flexible wind turbine blade which is mounted on a rigid test stand S. In O the test stand is elastically supported allowing for rotation only (see Figure 14). The strainless reference configuration is defined so that the blade reference axis R is horizontal and the blades cord is vertical near the tip.

The blade is 19 m long, its maximum cord length is 1.7 m and the trailing edge points upwards.

O and B are points on R, where B is a point on the blades root cross section and where $\overline{OB} = b$.

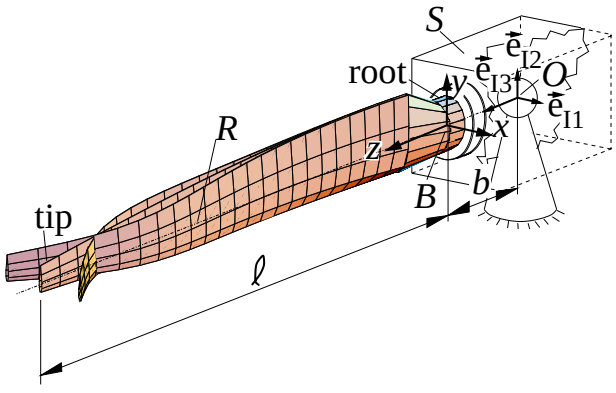

Figure 14: Sketch of the system. The system is shown three times in the same figure to illustrate a motion sequence of the blades second flapwise mode.

We use the expression “cross section” for all material points that make up the blades reference configuration in one plane perpendicular to R. “Profile” names the outer circumference of a cross section.

A motion is called ”flapwise” when it is predominantly horizontal, ”edgewise” refers to vertical motion and ”pitchwise” to cord rotation.

We differentiate between column matrix (an underlined symbol, e.g. $\underline{r}$) and vector (a bold faced symbol, e.g. $\mathbf{r}$). The column matrix is a triple of elements, the vector an element of the three dimensional space. Thus in $\mathbf{r} = \underline{r} \cdot \underline{\mathbf{e}}_I$ is $\mathbf{r}$ a position in space and $\underline{r}$ its coordinates in the coordinate system spanned by $\underline{\mathbf{e}}_I$, where $\underline{\mathbf{e}}_I$ holds the three unit vectors $\mathbf{e}_{I1}$, $\mathbf{e}_{I2}$, $\mathbf{e}_{I3}$. A twice underlined character is a matrix (e.g. $\underline{\underline{M}}$).

Rotation of the cross section about an axis in the cross sectional plane will be called tilt in order to differentiate between this bending related motion and a rotation about the longitudinal blade axis.

We allow for isotropic blade material only. Approaches accounting for the orthotropic laminate characteristics of rod material have been made (see [8]). But for our blade, only few informations were available about fiber directions, so the idea was dropped.

Principle of Virtual Work

We derive the equations of motion from the principle of virtual work:

$$\begin{aligned} \delta W &\stackrel{!}{=} 0 \\ &= \delta T + \delta U \ . \end{aligned} \tag{18}$$

where $\delta U = \int_V -\sigma_{ij}\ \delta\varepsilon_{ij}\ \mathrm{d}V$ is the virtual strain energy and $\delta T = \int_V -\varrho\ddot{\mathbf{r}} \cdot \delta\mathbf{r}\ \mathrm{d}V$ is the virtual work of d’Alembert forces. For simplicity the virtual work of gravitational and dissipative forces is not accounted for.

In the following sections it is important to remember that in the principle of virtual work a duality exists between forces and stresses on one hand and deflections and strains on the other. If we assume for example, that the main stresses in the cross sectional plain σ_{xx} and σ_{yy} can be neglected and be set to zero, then the respective (variations of the) strains are of no importance to us.

Kinematics

The unit vectors $(\mathbf{e}_{I1}, \mathbf{e}_{I2}, \mathbf{e}_{I3})^T := \underline{\mathbf{e}}_I$ form an orthogonal inertial right-hand coordinate system with $\mathbf{e}_{I1}, \mathbf{e}_{I3}$ spanning a horizontal plane (Figure 14). Transformation matrices $\underline{\underline{D}}_i(.)$ (see [11]) rotate the coordinate system $\underline{\mathbf{e}}_B$, which is attached to S, by angles $\kappa_i(t)$, $i = 1, 2, 3$ about O and

$$\underline{\mathbf{e}}_B(t) = \underline{\underline{D}}_3(\kappa_3(t))\underline{\underline{D}}_2(\kappa_2(t))\underline{\underline{D}}_1(\kappa_1(t))\ \underline{\mathbf{e}}_I \tag{19}$$

holds. The reference axis R and $\mathbf{e}_{B3}$ are parallel. R is not a particular axis (such as the connection of the centers of mass of all cross section would be), but is chosen with some arbitrariness.

B is the origin of the blades (x, y, z) coordinate system in the blade root. A material blade point $\{x, y, z\}$ is identified by its position vector in the undeformed reference configuration of the blade

$$\mathbf{r}_P^{(0)}(x, y, z) = x \cdot \mathbf{e}_{I1} + y \cdot \mathbf{e}_{I2} + (b + z) \cdot \mathbf{e}_{I3} \ . \tag{20}$$

The crucial question is, what blade deformations we account for and what coordinates we use to describe them. We introduce the chosen coordinates by following the material points of cross section z from their reference to the deflected configuration. We begin by introducing displacements $\underline{u} = (u_1(z,t),\ u_2(z,t),\ u_3(z,t))^T$ of point $\{0, 0, z\}$ on R in the $\underline{\mathbf{e}}_B$ coordinate system. Coordinate u_3 is the cross sections displacement in longitudinal blade direction (extension), u_1 and u_2 are the lateral displacements. The cross section is then tilted about $\mathbf{e}_{B1}$, subsequently about the resulting 2-axis and finally rotated (pitched) about the 3-axis. Using transformations $\underline{\underline{D}}_i$ from (19) again, the coordinate system attached to cross section z is

$$\underline{\mathbf{e}}_C(z,t) = \underline{\underline{D}}_3(\varphi_3(z,t))\underline{\underline{D}}_2(\varphi_2(z,t))\underline{\underline{D}}_1(\varphi_1(z,t))\ \underline{\mathbf{e}}_B \ , \tag{21}$$

thus that point $\{x, y, z\}$ from (20) holds at this point of the transformation the position

$$\mathbf{r}_P^{(1)}(x, y, z; t) = (b + z) \cdot \mathbf{e}_{B3} + \underline{u} \cdot \underline{\mathbf{e}}_B + (x, y, 0)^T \cdot \underline{\mathbf{e}}_C \ . \tag{22}$$

The displacement described by coordinates u_1, u_2, u_3, φ_1, φ_2, φ_3 is a rigid body motion of the cross section. Stopping at this point, we would end up with a Timoshenko beam model or, after further assumptions, an Euler-Bernoulli beam model and a separate torsional rod model.

Warping is an out of plane deformation of the cross section and is thus a function of x and y. It is an elastic coupling of torsion and flexure. With $\mathbf{e}_{C3}$ being perpendicular to the cross section defined by (22) and a chosen warping function

$$w(x, y, z; t) = \psi_1(z,t) \cdot xy + \psi_2(z,t) \cdot x^2 + \psi_3(z,t) \cdot y^2 \tag{23}$$

we find

$$\mathbf{r}_P(x, y, z; t) = \mathbf{r}_P^{(1)}(x, y, z; t) + w(x, y, z; t) \cdot \mathbf{e}_{C3} \ . \tag{24}$$

Linearization of (24) with respect to all dependent coordinates yields the displacement field $\Delta\mathbf{r}_P(x, y, z; t) = (\Delta r_x,\ \Delta r_y,\ \Delta r_z)^T \cdot \underline{\mathbf{e}}_I$ where

$$\begin{aligned}
\Delta r_x =& +(b + z) \cdot \kappa_2(t) - y \cdot \kappa_3(t) + u_1(z,t) - y \cdot \varphi_3(z,t), \\
\Delta r_y =& -(b + z) \cdot \kappa_1(t) + x \cdot \kappa_3(t) + u_2(z,t) + x \cdot \varphi_3(z,t), \\
\Delta r_z =& \quad y \cdot \kappa_1(t) - x \cdot \kappa_2(t) + u_3(z,t) + y \cdot \varphi_1(z,t) - x \cdot \varphi_2(z,t) \\
& \qquad + xy \cdot \psi_1(z,t) + x^2 \cdot \psi_2(z,t) + y^2 \cdot \psi_3(z,t) \ .
\end{aligned} \tag{25}$$

The warping function, defined in equation (23), can be interpreted as part of a Taylor series expansion of the cross section deflection in z-direction to second order in x and y.

Strain-displacement relation

With the displacement field (25) given, we compute the strains (see [14]) by

$$\begin{aligned}
\varepsilon_{xx}&=\frac{\Delta r_x}{\partial x}\ , \qquad & \varepsilon_{yz}&=\frac{1}{2}\left(\frac{\Delta r_z}{\partial y}+\frac{\Delta r_y}{\partial z}\right)=\varepsilon_{zy}\ ,\\
\varepsilon_{yy}&=\frac{\Delta r_y}{\partial y}\ , \qquad & \varepsilon_{zx}&=\frac{1}{2}\left(\frac{\Delta r_z}{\partial x}+\frac{\Delta r_x}{\partial z}\right)=\varepsilon_{xz}\ ,\\
\varepsilon_{zz}&=\frac{\Delta r_z}{\partial z}\ , \qquad & \varepsilon_{xy}&=\frac{1}{2}\left(\frac{\Delta r_x}{\partial y}+\frac{\Delta r_y}{\partial x}\right)=\varepsilon_{yx}\ .
\end{aligned} \tag{26}$$

Stress-strain relation

For a slender rod as the blade, we may assume that $\sigma_{yy} \equiv 0$, $\sigma_{zz} \equiv 0$. From the stress-strain-relations (Hook's law, see [14]), we obtain with modulus of elasticity E and modulus of shear G

$$\begin{aligned}
\sigma_{zz} &= E\varepsilon_{zz}\ , & \sigma_{xy} &= 2G\varepsilon_{xy},\\
\sigma_{xz} &= 2G\varepsilon_{xz}\ , & \sigma_{yz} &= 2G\varepsilon_{yz}.
\end{aligned} \tag{27}$$

Note that the stress-strain relations also yield the strains ε_{xx} and ε_{yy}. They could be used to compute the resulting in plane deformations of the cross section.

Form-functions

We choose polynomials in z as form-functions to describe the blade motion:

$$\begin{aligned}
u_i(z,t) &= \sum_{j=1}^{N(ui)} U_{ij}(t)\left(\frac{z}{\ell}\right)^j\ , \varphi_i(z,t) = \sum_{j=1}^{N(\varphi i)} \Phi_{ij}(t)\left(\frac{z}{\ell}\right)^j\ ,\\
\psi_i(z,t) &= \sum_{j=1}^{N(\psi i)} \Psi_{ij}(t)\left(\frac{z}{\ell}\right)^j\ .
\end{aligned} \tag{28}$$

Other form-functions such as Legendre-type polynomials are more appropriate, but are not employed here for the sake of simplicity. The time dependent coefficients of the form-functions are the coordinates of the blade model.

Definition of blade geometry and system parameters

We define the blade geometry by a number of generating cross sections of different size and shape. Each of them consists of the same number of tetragons (see Figure 15).

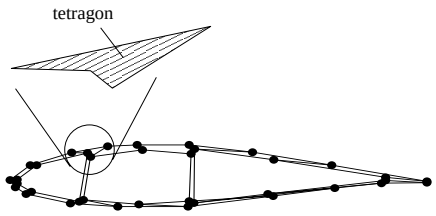

Figure 15: Definition of cross sections with tetragons. Dots mark the points, which define the edges of the tetragons.

Connecting the edges of a tetragon with the respective element on a neighboring cross section defines a polyeder - which is one “volume element” of the blade.

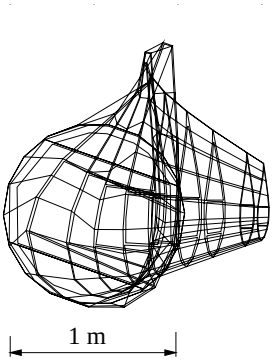

Figure 16: Discretization of the blade geometry.

Figure 16 shows the geometry of the blade with generating cross sections and connecting lines. For clarity, the blade tip is deflected 1 m flapwise out of its reference configuration (the blade is straight in its reference configuration).

For simplicity, and lack of detailed information, all polyeders are assumed to consist of material having the same modulus of elasticity and shear and the same material density. The rotational stiffness and moment of inertia of the support with respect to κ_1, κ_2 and κ_3, are estimated to $k_S = 10^8$ Nm and $J = 10^3$ kg m^2 respectively.

Using (25), (26), (27), the virtual work (18) for a polyeder can be given as a function of $u_i(z,t)$, $\varphi_i(z,t)$, $\psi_i(z,t)$ and their derivatives using a computer algebra program (Mathematica). Since the generating cross sections are parallel, the integral can be solved over x and y so it depends of z and the parameters of the polyeder points.

We derive the elements of the stiffness matrix numerically. As an example, we derive in the equation of motion for $\Psi_{i,j}$ (see equation(28)) the coefficient of $U_{k,l}$. In δW we set $U_{k,l}(t) = 1$ m and $\delta\Psi_{i,j} = 1$. All other coordinates, their variations and time derivatives are set to zero. The numerical solution of the integral of the virtual work over all polyeders yields the respective element of the stiffness matrix.

Slaving warping, extension and tilt to the remaining coordinates

From the solution of integral (18) over the blade volume we obtain a system of linear differential equations

$$\begin{pmatrix} \underline{\underline{M}}_{ZZ} & \underline{\underline{M}}_{ZQ} \\ \underline{\underline{M}}_{QZ} & \underline{\underline{M}}_{QQ} \end{pmatrix} \begin{pmatrix} \ddot{\underline{Z}} \\ \ddot{\underline{Q}} \end{pmatrix} + \begin{pmatrix} \underline{\underline{K}}_{ZZ} & \underline{\underline{K}}_{ZQ} \\ \underline{\underline{K}}_{QZ} & \underline{\underline{K}}_{QQ} \end{pmatrix} \begin{pmatrix} \underline{Z} \\ \underline{Q} \end{pmatrix} = \underline{0} \qquad (29)$$

where $\underline{Z} = \{U_{11}, \ldots, U_{1N(u1)}, U_{21}, \ldots, U_{2N(u2)}, \Phi_{31}, \ldots, \Phi_{3N(\varphi 3)}\}$ and $\underline{Q} = \{U_{31}, \ldots, U_{3N(u3)}, \Phi_{11}, \ldots, \Phi_{1N(\varphi 1)}, \Psi_{11}, \ldots, \Psi_{3N(\psi 3)}\}$. $\underline{Z}$ holds the dependent coordinates, which are essential for the description of the blades flexure and torsion. $\underline{Q}$ dominates eigenmodes in a very high frequency range - which we are not interested in - and contributes to the lower frequency modes by a kind of forced swerving movement only. In physical systems, where damping is always present, their modes decay very rapidly and do not contribute to the solution of interest. For the solution of the equations of motion – especially when solving it as an initial value problem – it is most desirable to eliminate these coordinates.

We choose to neglect the virtual work of d'Alembert forces related to $\underline{Q}$. For a slender beam, their inertia terms do not contribute significantly to the flexural and torsional motion of the blade. We set

$$\underline{\underline{M}}_{ZQ} = \underline{\underline{M}}_{QZ} = \underline{\underline{0}} \quad \text{and} \quad \underline{\underline{M}}_{QQ} = \underline{\underline{0}}$$

and thus slave $\underline{Q}$ to $\underline{Z}$ by

$$\underline{Q} = -\underline{\underline{K}}_{QQ}^{-1} \underline{\underline{K}}_{QZ} \underline{Z} \,. \qquad (30)$$

Introduction of (30) in (29) yields

$$\underline{\underline{M}}_{ZZ} \ddot{\underline{Z}} + \underbrace{\left(\underline{\underline{K}}_{ZZ} - \underline{\underline{K}}_{ZQ} \underline{\underline{K}}_{QQ}^{-1} \underline{\underline{K}}_{QZ} \right)}_{=: \underline{\underline{K}}^*} \underline{Z} = \underline{0} \,. \qquad (31)$$

The equations of motion are solved as an eigenvalue problem.

4.2 Comparing model and experiment

Blade model

For the mathematical model used in the following comparison, we set the number of form-functions to

$$N(u_3) = N(\varphi_1) = N(\varphi_2) = N(\psi_i) = 10, \; i = 1, 2, 3$$

and

$$N(u_1) = N(u_2) = N(\varphi_3) = 8 \,.$$

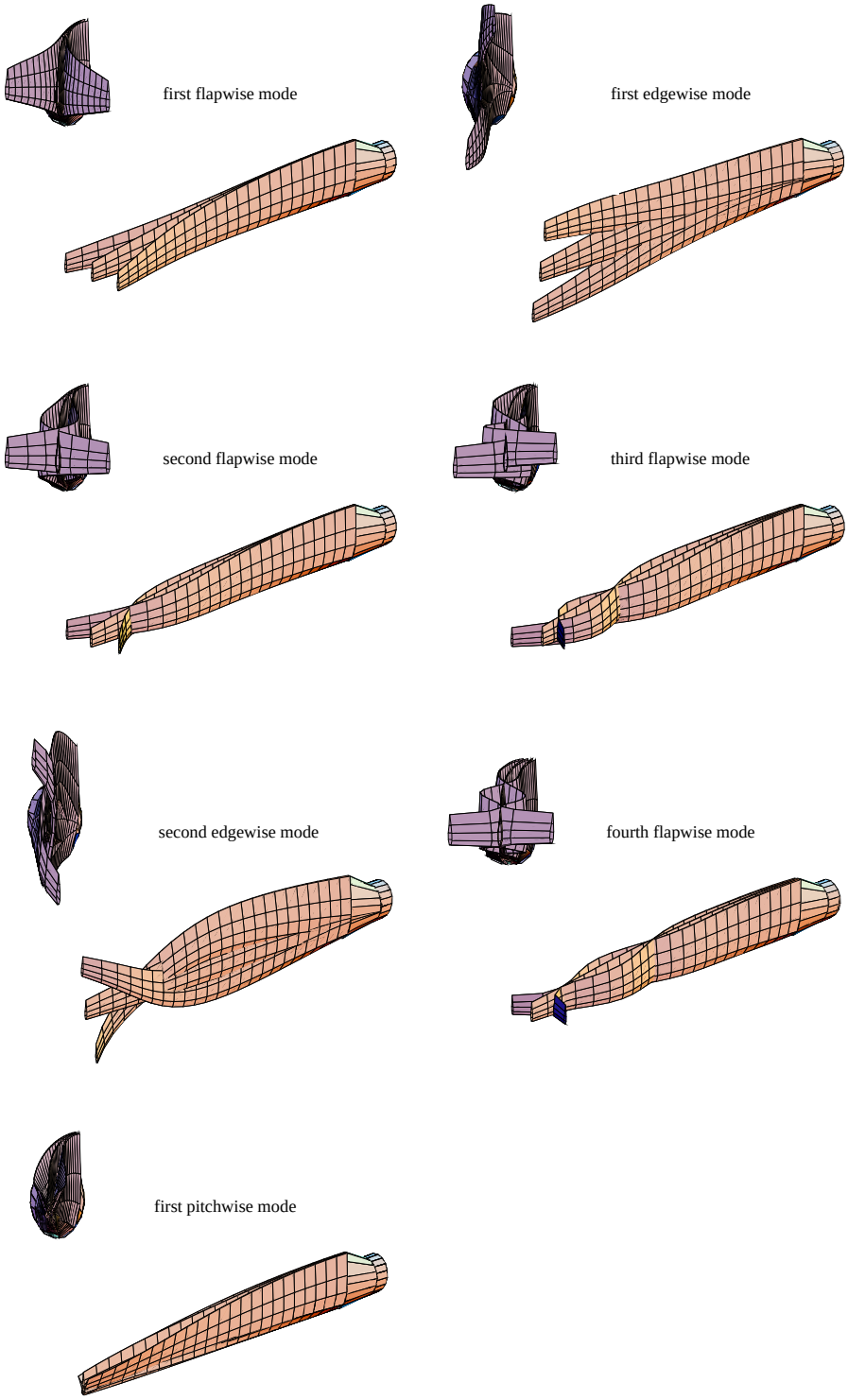

Figure 17: Computed mode shapes.

Experiments

The experimental modal analysis [15] was performed using three charge accelerometers for each of ten cross sections of the blade between tip and root. The blade was excited with a hammer at $z = 11.3$ m, the hammer force $f(t)$ was measured and the frequency response functions were obtained. Modal mass, damping, stiffness, eigenfrequencies and mode shapes were identified.

Comparison

Table 1 compares measured and computed eigenfrequencies. The mode name describes the predominant motion of the blade.

Table 1. Comparison of measured and computed eigenfrequencies.

mode name	1^{st} flap	1^{st} edge	2^{nd} flap	3^{rd} flap	2^{nd} edge	4^{th} flap	1^{st} pitch
measured e.f./Hz	1.64	2.94	4.91	9.73	10.62	16.25	22.87
computed e.f./Hz	1.60	3.06	5.01	10.07	11.90	17.02	22.31

The eigenfrequencies approximate the experimentally found results much better then could be expected from a modeling that had to deal with many uncertainties in the system parameters. The mode shapes however do not fit as well:

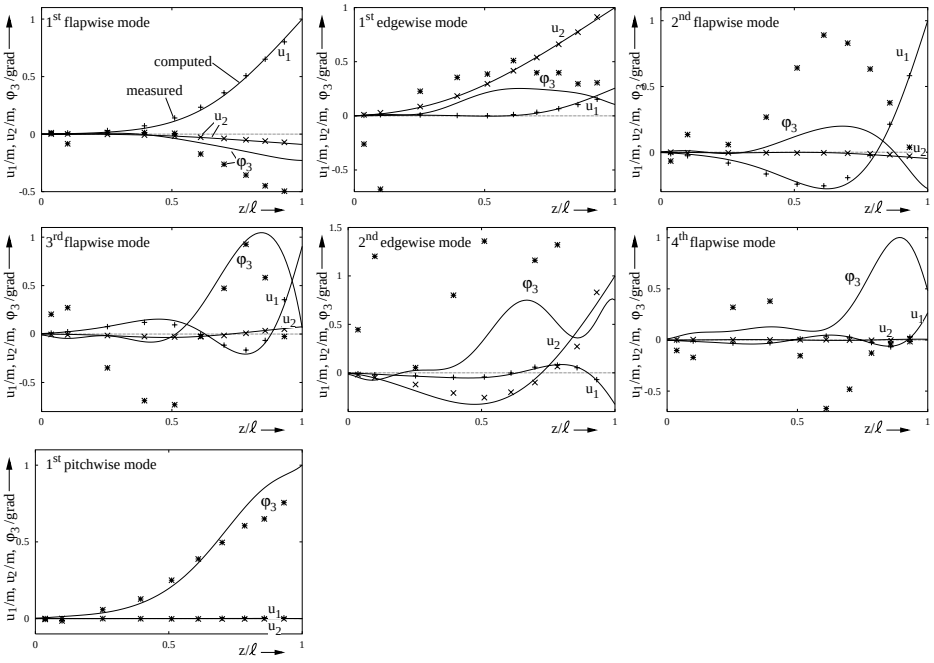

Figure 18: Comparison of measured and computed mode shapes.

The free multiplier in the measured modeshapes – which scales the blades deflection but leaves the relation between u_1, u_2, φ_3 unchanged – was set as to minimize the difference between measured and computed edge- and flapwise deflections.

The influence of warping

Finally, we investigate the influence of warping on the modes. Figure 19 shows the computed eigenfrequencies for the model over the number $N(\psi_i)$, $i = 1, 2, 3$ of form-functions used for the discretization of the warping function.

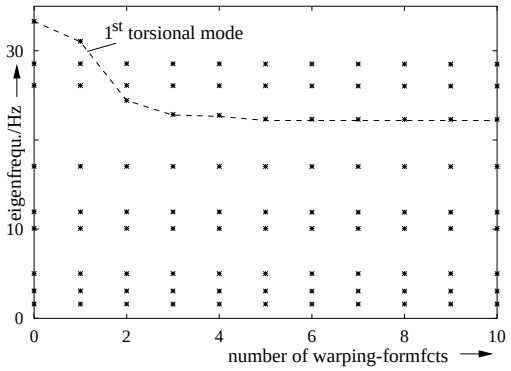

Figure 19: Computed eigenfrequencies of the blade over the number of form-functions for ψ_i.

As $N(\psi_i) < 4$, the first pitch-eigenfrequency increases significantly. But already at higher numbers of $N(\psi_i)$, the relation in the mode shapes between φ_3 on one hand and u_1, u_2 on the other hand changes.

4.3 Conclusion

A rod model for slender, tapered, closed structures is presented and applied to a wind turbine blade. The mathematical model is solved as an eigenvalue problem and results are compared with an experimental modal analysis.

Even though the general model characteristics (position of nodes, direction of motion) match quite well, the cord rotation is for some modeshapes significantly underestimated. The question remains, what assumptions in the modeling process are the main sources of these differences (e.g. anisotropic material, geometry, order of Taylor series expansion in x and y, ...).

Nevertheless the mathematical model presented is a serious alternative to commercial FE methods when computing first estimates for eigenfrequencies and modal shapes. The very few degrees of freedom allow applications for systematic stability investigations and fast solution as an initial value problem. Due to its semi-analytic nature, the model can - and has been - extended to allow for rotation of the whole blade and the computation of gyroscopic terms (e.g. centrifugal stiffening) and periodic coefficients.

5 Identification of the Stiffness-Matrix for a Simple Blade Model from ANSYS-Solutions

Due to complicated deformation mechanisms of a wind turbine blade (for example warping and anisotropic material properties) are individual cross-section motions like rotation and flexure elastically coupled. FE-models, based on shell elements, allow a very detailed description of these mechanisms, but the resulting model uses too many degrees of freedom to be used in systematic investigations such as parameter studies.

5.1 Assumptions

The following approach assumes the mathematical blade model on the form

$$\underline{\underline{M}}\,\ddot{\underline{p}} + \underline{\underline{K}}\,\underline{p} = \underline{0} \tag{32}$$

with $\underline{\underline{M}}, \underline{\underline{K}} \in I\!R^{K\times K}$, $K = 9$ and $\underline{p}$ being the row matrix of all dependent coordinates. $\underline{\underline{M}}$ can relatively easy be computed from the blade geometry and the material density whereas $\underline{\underline{K}}$ is identified from eigenvalues and eigenvectors known from FEM-computations with ANSYS.

5.2 Kinematics

The local coordinate system $\{x, y, z\}$ lies in an inertial system with its x-axis on the blades reference axis R. The R-axis is defined to be the line connecting the quarter cord points of all cross section.

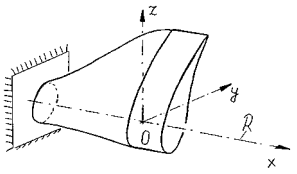

Figure 20: The blade coordinate system.

Let translations of R in y- and z-directions be $u_2(x,t)$ and $u_3(x,t)$, respectively, and rotation of the cross section x around R be $\varphi_1(x,t)$.

When the blade is in its strainless reference configuration, a point P has coordinates $\underline{r}^{P,ref} = \{x, y, z\}$. In the blades deformed configuration its position is described by

$$\underline{r}^{P} = \{x, u_2(x,t) + y + z\cdot\varphi_1(x,t), u_3(x,t) + z - y\cdot\varphi_1(x,t)\} \tag{33}$$

for small φ_1.

The form-functions chosen for $u_2(x,t)$, $u_3(x,t)$ and $\varphi_1(x,t)$ are

$$\begin{aligned} u_2(x,t) &= \sum_{n=1}^{N_{u2}} U_{2j} \left(\frac{x}{\ell}\right)^j, \\ u_3(x,t) &= \sum_{n=1}^{N_{u3}} U_{3j} \left(\frac{x}{\ell}\right)^j \text{and} \\ \varphi_1(x,t) &= \sum_{n=1}^{N_{\varphi 1}} \Phi_{1j} \left(\frac{x}{\ell}\right)^j. \end{aligned} \tag{34}$$

Dependent coordinates of our model are thus

$$\underline{p}(t) = \left\{ U_{21}(t), \ldots, U_{2N_{u2}}(t), U_{31}(t), \ldots, U_{3N_{u3}}(t), \Phi_{11}(t), \ldots, \Phi_{1N_{\varphi 1}(t)} \right\} .$$

5.3 Equations of motion

With the principle of virtual work, the equations of motion are

$$\begin{aligned} \delta W &= \delta W^{kin} + \delta W^{ela} \\ &\stackrel{!}{=} 0 \end{aligned}$$

with the virtual work of d'Alembert forces δW^{kin} and the virtual elastic energy δW^{ela}.

With the simple kinematics that we allow for the blade, an elastic coupling between the individual motions (u_2, u_3, φ_1) can not directly be derived. The stiffness matrix is therefore derived from an ANSYS FEM solution as described later.

5.4 Mass matrix

The mass matrix comes from the virtual work of d'Alembert forces

$$\delta W^{kin} = \int_M -\ddot{\underline{r}}^P \cdot \delta \underline{r}^P \mathrm{d}M \tag{35}$$

where $\delta \underline{r}^P$ is the virtual displacement of P chosen as in (34) and M is the blade mass.

We introduce the form-functions for displacements and virtual displacements into (35) and are faced with the cumbersome task to solve the integral over M. Using the FE mesh generated with ANSYS, we can simplify this task.

Let N be the number of finite elements in ANSYS and V_n be the volume of element n, and ϱ_n its density. We write

$$\delta W^{kin} = \sum_{n=1}^{N} \int_{V_n} -\varrho_n \ \ddot{\underline{r}}^P \cdot \delta \underline{r}^P \mathrm{d}V \tag{36}$$

which reads for shell elements with element wise constant shell-thickness h_n and shell area A_n

$$\delta W^{kin} = \sum_{n=1}^{N} \underbrace{\int_{A_n} -\varrho_n h_n \ \underline{\ddot{r}}^P \cdot \delta \underline{r}^P \mathrm{d}A}_{=: \delta W_n^{kin}} \ . \tag{37}$$

The ANSYS shell elements used have triangular form with corner coordinates $\underline{c}_1 = \{x_1, y_1, z_1\}$, $\underline{c}_2 = \{x_2, y_2, z_2\}$ and $\underline{c}_3 = \{x_3, y_3, z_3\}$. On element basis, we introduce the $\{\xi_1, \xi_2, \xi_3\}$-coordinate system, such that ξ_1 and ξ_2 span the shell centerplane defined by $\underline{c}_1$, $\underline{c}_2$ and $\underline{c}_3$ (see Figure 21) and ξ_3 is the coordinate perpendicular to the shell centerplane.

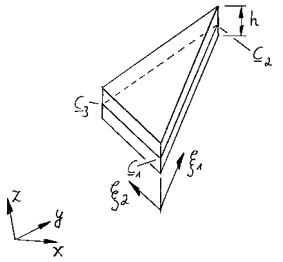

Figure 21: Finite element and local coordinates ξ_1, ξ_2.

Then the inertial coordinates are $x = x(\xi_1, \xi_2, \xi_3)$, $y = y(\xi_1, \xi_2, \xi_3)$ and $z = z(\xi_1, \xi_2, \xi_3)$ with relations

$$\begin{array}{ll} \{x(0,0,0), y(0,0,0), z(0,0,0)\} := \underline{c}_1 & , \\ \{x(1,0,0), y(1,0,0), z(1,0,0)\} := \underline{c}_2 & \text{and} \\ \{x(0,1,0), y(0,1,0), z(0,1,0)\} := \underline{c}_3 & . \end{array}$$

Thus, the element integral (37) can be written as an integral of ξ_1 and ξ_2. From (33) we find

$$\underline{\ddot{r}}^P \cdot \delta \underline{r}^P = (\delta u_2, \delta u_3, \delta \varphi_1) \begin{pmatrix} 1 & 0 & \tilde{z} \\ 0 & 1 & -\tilde{y} \\ \tilde{z} & -\tilde{y} & (\tilde{y}^2 + \tilde{z}^2) \end{pmatrix} \begin{pmatrix} \ddot{u_2} \\ \ddot{u_3} \\ \ddot{\varphi}_1 \end{pmatrix} \tag{38}$$

with $\tilde{y} = y(\xi_1, \xi_2, 0)$ and $\tilde{z} = z(\xi_1, \xi_2, 0)$. To simplify integration over A_n, we use the ANSYS-discretization of the motion of the structure into form-functions on triangular shell elements

$$\begin{aligned} u_2(x,t) = \tilde{u}_2(\xi_1, \xi_2, t) = {} & u_{21}(t) \cdot (1 - \xi_1\ ) \cdot (\ 1 - \xi_2\ ) + \\ & u_{22}(t) \cdot \quad \xi_1\ \cdot (\ 1 - \xi_2\ ) + \\ & u_{23}(t) \cdot (1 - \xi_1\ ) \cdot \quad \xi_2 \end{aligned}$$

and likewise for u_3 and φ_1.

We abbreviate

$$\begin{array}{rl} \underline{p}(t) = & \{u_{21}(t), u_{22}(t), u_{23}(t), u_{31}(t), u_{32}(t), u_{33}(t), \varphi_{11}(t), \varphi_{12}(t), \varphi_{13}(t)\} \\ & \text{and} \\ \delta \underline{p} = & \{\delta u_{21}, \delta u_{22}, \delta u_{23}, \delta u_{31}, \delta u_{32}, \delta u_{33}, \delta \varphi_{11}, \delta \varphi_{12}, \delta \varphi_{13}\} \ . \end{array}$$

Then (37) reads

$$\begin{aligned}\delta W_n^{kin} &= \int_{\xi_1=0}^{1}\int_{\xi_2=0}^{1-\xi_1} -\varrho_n h_n \;\; \delta\underline{p}\,\underline{\underline{m}}\,\ddot{\underline{p}}\;|J|\;\mathrm{d}\xi_2\mathrm{d}\xi_1 \\ &= \qquad\qquad \delta\underline{p}\,\underline{\underline{M}}_n\,\ddot{\underline{p}}\end{aligned}$$

with J being the Jacobian between $\{x, y, z\}$ and $\{\xi_1, \xi_2, \xi_3\}$ and $\underline{\underline{m}}$ resulting from (38). Finally, we find

$$\underline{\underline{M}} = \sum_{n=1}^{N} \underline{\underline{M}}_n \; .$$

5.5 Stiffness matrix

From ANSYS, we obtain eigenfrequencies ω_i and eigenvectors of the blade. We sort the solutions with respect to the positive eigenfrequencies ω_i, so that $\omega_i < \omega_{i+1}$.

We are now trying to describe the ANSYS eigenmodes of lowest eigenfrequency with our form-functions from (34).

The ANSYS solution defines the motion of point P in the form $\underline{u}_A^P(x, y, z, t) = \underline{\hat{u}}_A^P(x, y, z)\cos(\omega_i t)$. Likewise, our form-functions (34) give, for $\underline{p}(t) = \underline{\hat{p}}\cos(\omega_i t)$ and some approximation $\underline{\hat{p}}$ of an eigenmode, the motion of point P to be $\underline{u}_G^P(\underline{\hat{p}}, x, y, z, t) = \underline{\hat{u}}_G^P(\underline{\hat{p}}, x, y, z)\cos(\omega_i t)$.

With

$$\underline{f} := \underline{\hat{u}}_A^P - \underline{\hat{u}}_G^P,$$

we define an error

$$F := \int_V \underline{f}\cdot\underline{f}\; dV$$

and minimize F with respect to $\underline{\hat{p}}$. For simplicity, we take

$$\begin{aligned} F \approx \tilde{F} \qquad &= \qquad \sum_{n=1}^{N} \underline{f}_n \cdot \underline{f}_n \\ &\stackrel{!}{=} \qquad \min\,, \end{aligned}$$

where $\underline{f}_n$ is the difference in nodal displacements in the FE nodes.

This procedure gives an approximation $\underline{\hat{p}}_i$ for each ANSYS-eigenmode i.

In Figure 22, the identified eigen-forms are plotted. For the identification, $N_{u2} = 8$, $N_{u3} = 8$ and $N_{\varphi_1} = 6$ were used.

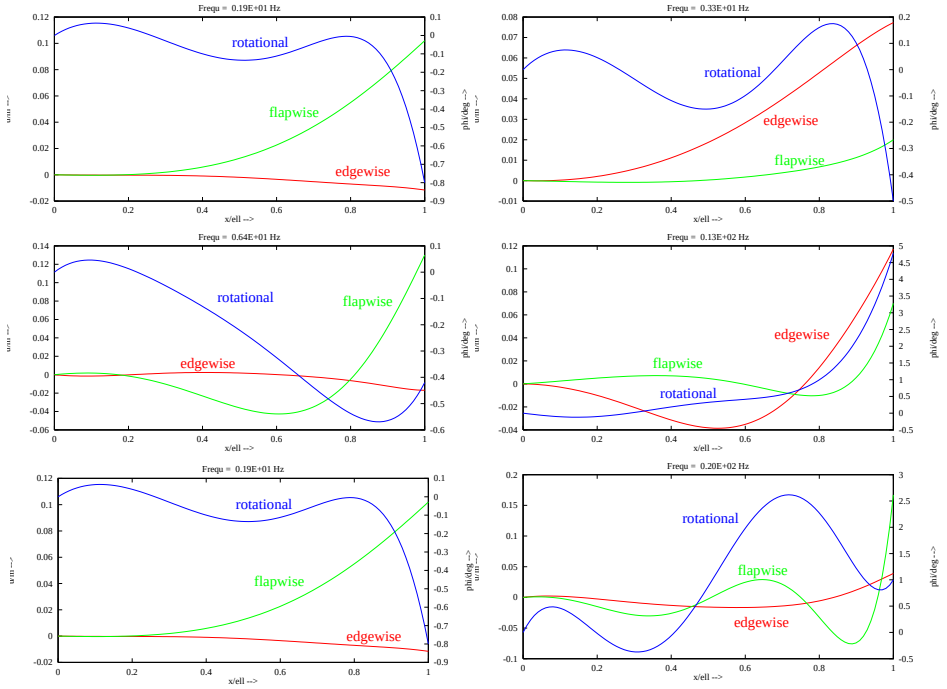

Figure 22: Eigenmodes identified from ANSYS-Solutions.

From (32), we get

$$\underline{\underline{K}}\,\underline{\hat{p}}_i = \underbrace{\omega_i^2\,\underline{\underline{M}}\,\underline{\hat{p}}_i}_{=:\,\underline{\hat{r}}_i}\,,$$

where the elements of $\underline{\underline{K}}$ are unknown.

Let $\underline{\underline{P}} = \{\underline{\hat{p}}_1, \ldots, \underline{\hat{p}}_9\}$ and $\underline{\underline{R}} = \{\underline{\hat{r}}_1, \ldots, \underline{\hat{r}}_9\}$, then the resulting equation to solve is

$$\underline{\underline{K}}\,\underline{\underline{P}} = \underline{\underline{R}}\,.$$

Unless $\underline{\underline{P}}$ is singular, this equation can be solved for $\underline{\underline{K}}$. The procedure has been implemented in a FORTAN program, and a state-of-the-art optimization routine has been used. Comparisons with the model from section 4 shows good agreement of the matrices.

5.6 Conclusion

A mathematical model for a wind turbine blade with very few degrees of freedom is presented, where the models stiffness matrix is derived from ANSYS solutions. The model shall be used in engineering models to allow for systematic stability investigations (flutter).

6 A Word on Damping

Problem Statement

For simplicity, structural damping (here for the one-dimensional case) is mostly modelled by

$$\sigma = E_0\Big(\varepsilon + \beta\dot{\varepsilon}\Big) \qquad (\text{"Rayleigh-damping"})$$

with damping coefficient β. For harmonic excitation $\varepsilon = \hat{\varepsilon}\sin(2\pi\, f\, t)$, the relation

$$\hat{\sigma} = \Big(E'_R + \jmath E''_R\Big)\hat{\varepsilon} \text{ where } \jmath = \sqrt{-1}$$

is found with $E'_R = E_0$, $E''_R = 2\pi E_0 \beta f$.

For most materials, this model appears to be inappropriate for "high" frequencies f:

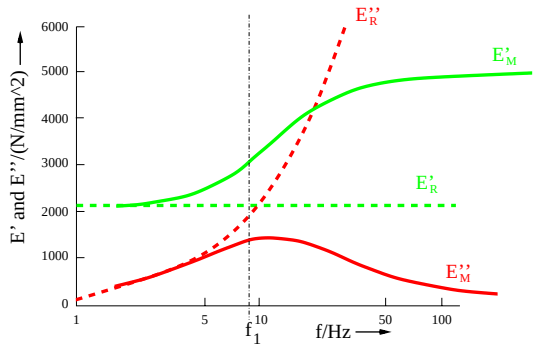

Figure 23: Measured moduli E'_M, E''_M for Plexiglas and E'_R, E''_R.

Problem: Find the limit frequency f_1, up to which the Rayleigh-model is valid.

If for blade materials, f_1 is small compared to relevant eigenfrequencies of a wind turbine, try to find an appropriate model for structural damping.

Models with Inner Variables

A mathematical damping model with only one inner variable δ is sketched in Figure 24 and is compared with the Rayleigh model. Note, that δ is an additional degree of freedom!

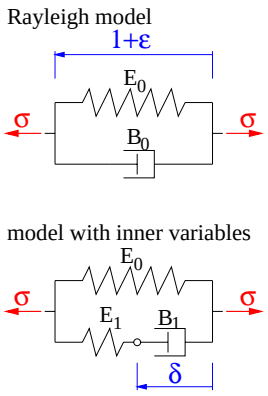

Figure 24: Phenomenological interpretation of damping models.

From Figure 24 we read

$$\sigma = E_0\varepsilon + E_1\,(\varepsilon - \delta) \;\text{ and }\; E_1\,(\varepsilon - \delta) = B_1\dot{\delta}\;.$$

With $\varepsilon = \hat{\varepsilon}\sin(\Omega t)$, $B_1 = \beta E_1$ and $E_1 = \alpha E_0$ we find

$$\frac{\hat{\sigma}}{\hat{\varepsilon}} = \underbrace{\frac{(1+(1+\alpha)\beta^2\Omega^2)E_0}{1+\beta^2\Omega^2}}_{E_I'} + \jmath\underbrace{\frac{\alpha\beta\Omega E_0}{1+\beta^2\Omega^2}}_{E_I''}$$

For $\alpha = 0.2$ and $\beta = 0.01$ the relation $\hat{\sigma}/\hat{\varepsilon}$ is plotted over frequency f in Figure 25.

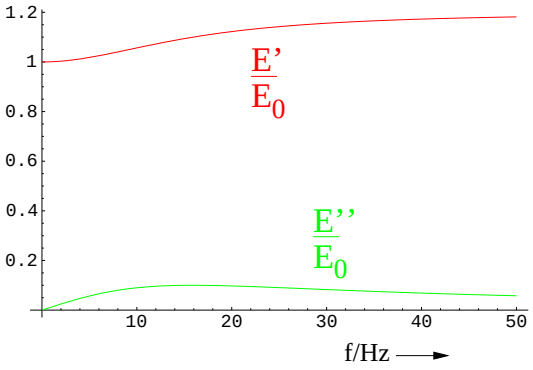

Figure 25: Moduli E' and E'' of model with one inner Variable.

Please note, that the abscissa values have logarithmic spacing in Figure 24 and linear spacing in Figure 25.

The theory of mathematical damping models using inner variables is described in [1].

Note that the equations of motion are still linear! An eigenvalue-analyses with a model using inner variables can be performed as usual. The number of state variables increases though. For δ, an extra linear differential equation of first order is obtained.

7 Creaking Doors – a Stability Problem

For autonomous, linear, ordinary differential equations, nobody would bother to compute solutions in the time domain because eigenvalues give complete information about the system.
For nonlinear differential equations, no such general way exists to condense informations about the system dynamics. Each new set of initial values in a time integration might give a solution with a whole new character.

7.1 Stability Considerations

A first approach is to find out, if certain desired "smooth" solutions can be observed in real systems (see Figure 26). We will call such a smooth solution a reference solution, and if it can be realized is decided by stability.

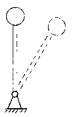

Figure 26: One reference solution for a pendulum.

For a creaking door, we present the solution procedure for linear stability analysis. In section 7.3, this procedure is applied numerically.

7.2 Solution Procedure

Opening an unoiled door produces a creaking sound.

The door redirects the global opening motion into a local process: the dry hinge steers the flow of energy, so that it self-sustains local, high frequency oscillations.

This is called self-excitation.

The interesting point is that the door does not creak, when it is opened fast. Thus, for self-excitation of a door its parameters $\underline{p} = \{p_1, \ldots, p_M\}^T$ (mass, friction characteristic, etc.) **and** its state $\underline{x} = \{x_1, \ldots, x_N\}^T$ (speed, deflection) decide upon creaking.

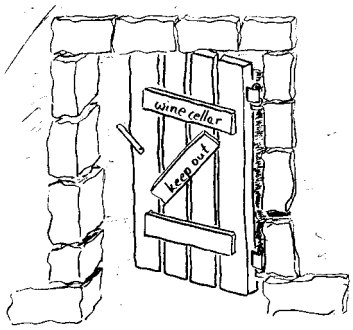

Figure 27: Creaking door.

Sneeking into a wine-cellar, we are not really interested in the details of the door-motion, but if it creaks or not. The underlying question is stability.

Stability is the property of a system to move towards some close-by reference solution. The reference solution for the door is its stationary rotation around the hinges as we pull the handle. Creaking means, the door oscillates as an elastic body around the stationary rotation. This reference solution is then unstable.

A mathematical stability analysis has its roots in the system of nonlinear, ordinary differential equations of motion for the door:

$$\dot{\underline{x}} = \underline{f}(\underline{x}, \underline{p}), \text{ where } \begin{array}{ll} \underline{x}(t) & \text{is the column matrix of the state variables,} \\ \underline{p} & \text{is the column matrix of all system parameters and} \\ \underline{f} & \text{is a nonlinear function .} \end{array} \tag{39}$$

Let the stationary rotation (the reference solution) of the door be characterized by $\dot{\underline{x}} \equiv 0$. Then

$$\underline{0} = \underline{f}(\underline{x}^*, \underline{p}) \tag{40}$$

is the nonlinear system of equations for the reference solution $\underline{x}^*$.

What happens, if we slightly disturb $\underline{x}^*$, say $\tilde{\underline{x}}(t) = \underline{x}^* + \underline{\xi}(t)$?

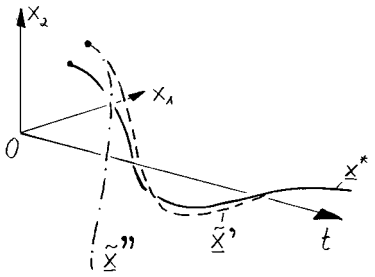

Figure 28: Reference solution $\underline{x}^*$ and neighbouring solution $\tilde{\underline{x}}$.

If $\underline{\xi}(t)$ grows ($\tilde{\underline{x}}''$ in Figure 28), $\underline{x}^*$ is unstable, if it decays ($\tilde{\underline{x}}'$), $\underline{x}^*$ is stable.

If we agree to stay very close to the reference solution, we may linearize $\underline{f}$ about $\underline{x}^*$:

$$\underline{f}(\underline{x}, \underline{p}) \approx \underline{f}(\underline{x}^*, \underline{p}) + \{ \left. \frac{\partial f_i}{\partial x_j} \right|_{\underline{x} = \underline{x}^*} \cdot \xi_j(t) \} \tag{41}$$

and write (39) in linear form as

$$\dot{\underline{\xi}} = \underline{\underline{A}}(\underline{p})\, \underline{\xi}, \text{ with matrix elements } a_{ij} = \left. \frac{\partial f_i}{\partial x_j} \right|_{\underline{x} = \underline{x}^*} . \tag{42}$$

It has solutions

$$\underline{\xi}(t) = \sum_{n=1}^{N} \hat{\underline{\xi}}_n \mathrm{e}^{\lambda_n t} \tag{43}$$

with eigenvectors $\hat{\underline{\xi}}_n$ and eigenvalues λ_n. So the question is, if at least one eigenvalue has a positive real part, $\Re(\lambda_n) > 0$, which means instability.

The result is a stability map for example over prescribed opening speed, Ω, and oiling condition, o, of the hinges. For each combination (Ω, o) a reference solution $\underline{x}^*$ is computed from (40) and the eigenvalue problem associated with (42) is solved. If for a set (Ω_k, o_k) one $\Re(\lambda_{k,n}) > 0$ exists (the reference solution associated with (Ω_k, o_k) is unstable), then a red dot is drawn in the map, a green one otherwise.

The result might look as follows:

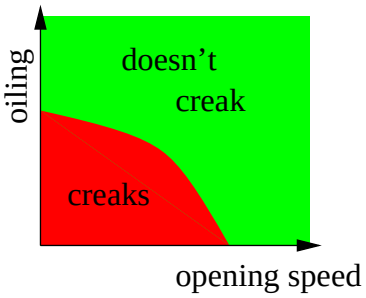

Figure 29: Stability of stationary door rotation.

For poor oiling and slow opening, the door creaks.

7.3 Numerical Realization

We derive equations of motion for the simplified door sketched in Figure 30. The door handle is rotated with constant angular velocity Ω around the hinges, the deflection of the door from its plane reference configuration be $w(r,t)$, where $r \in [0, \ell]$ is the radial coordinate from hinge to handle.

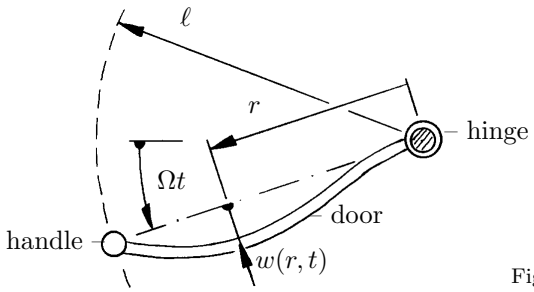

Figure 30: Sketch of the door seen from above.

We derive equations of motion with the principle of Hamilton-Ostrogradskij, which states

$$\delta \int_{t_1}^{t_2} \Big(T - U \Big) \mathrm{d}t + \tilde{\delta} W = 0 \,,$$

where T and U are kinematic and potential energy respectively, δ is the variation operator and $\tilde{\delta} W$ is the virtual work of nonconservative forces.

With mass per unit length μ and bending stiffness EI of the door is

$$T = \int_0^\ell \frac{1}{2}\mu\Big(\Omega r + \dot{w}(r,t)\Big)^2 \mathrm{d}r + \text{ small terms}$$

and

$$U = \int_0^\ell \frac{1}{2} EI\ w''(r,t)^2 \mathrm{d}r\ .$$

$\tilde{\delta}W$ is the virtual work of the friction moment M in the hinges and of material damping (damping coefficient β) with respect to virtual displacements $\tilde{\delta}w(r)$:

$$\tilde{\delta}W = \int_0^\ell \beta EI\ w''(r,t) \cdot \tilde{\delta}w''(r)\mathrm{d}r + M \cdot \tilde{\delta}w'(0)\ .$$

The friction moment M is a nonlinear function of the rotation velocity $\omega\ :=\ \Omega + \dot{w}'(0,t)$.

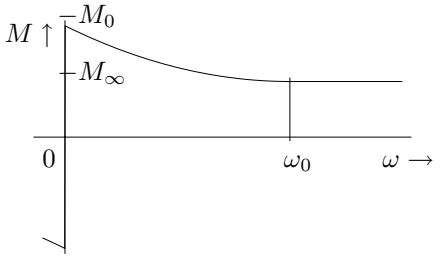

Figure 31: Friction moment $M(\omega)$.

The principle of Hamilton-Ostrogradskij is a very elegant and easy way to derive equations of motion for systems of elastic bodies. We simply choose admissible form-functions for the deformations of the door, integrate over the door width ℓ, and the principle assures that, for the given discretisation, we get an optimal solution.

The form-functions have to fulfill only the geometric boundary conditions

$$w(0,t) = 0 \text{ and } w(\ell,t) = 0\ .$$

An admissible form-function is

$$w(r,t) = \frac{(\ell - r)r\Big((\ell - r)W_0(t) - rW_\ell(t)\Big)}{\ell^2}$$

with two degrees of freedom $W_0(t) = w'(0,t)$ and $W_\ell(t) = w'(\ell,t)$. We obtain two differential equations

$$\underbrace{\mu\frac{\ell^3}{5}\begin{pmatrix} \frac{1}{21} & -\frac{1}{28} \\ -\frac{1}{28} & \frac{1}{21} \end{pmatrix}}_{=:\,\underline{\underline{M}}} \cdot \begin{pmatrix} \ddot{W}_0 \\ \ddot{W}_\ell \end{pmatrix} + \underbrace{\beta\frac{2EI}{\ell}\begin{pmatrix} 2 & 1 \\ 1 & 2 \end{pmatrix}}_{=\,\beta\underline{\underline{K}}} \cdot \underbrace{\begin{pmatrix} \dot{W}_0 \\ \dot{W}_\ell \end{pmatrix}}_{=:\,\underline{V}}$$

$$+ \underbrace{\frac{2EI}{\ell}\begin{pmatrix} 2 & 1 \\ 1 & 2 \end{pmatrix}}_{=\,\underline{\underline{K}}} \cdot \underbrace{\begin{pmatrix} W_0 \\ W_\ell \end{pmatrix}}_{=:\,\underline{W}} = \underbrace{\begin{pmatrix} M(\omega) \\ 0 \end{pmatrix}}_{=:\,\underline{m}} \qquad (44)$$

or

$$\underbrace{\begin{pmatrix} \underline{\underline{M}} & \underline{\underline{0}} \\ \underline{\underline{0}} & \underline{\underline{E}} \end{pmatrix}}_{=:\,\underline{\underline{Q}}_1} \cdot \begin{pmatrix} \dot{\underline{V}} \\ \dot{\underline{W}} \end{pmatrix} + \underbrace{\begin{pmatrix} \beta\underline{\underline{K}} & \underline{\underline{K}} \\ -\underline{\underline{E}} & \underline{\underline{0}} \end{pmatrix}}_{=:\,\underline{\underline{Q}}_2} \cdot \underbrace{\begin{pmatrix} \underline{V} \\ \underline{W} \end{pmatrix}}_{=:\,\underline{x}} = \underbrace{\begin{pmatrix} \underline{m} \\ \underline{0} \end{pmatrix}}_{=:\,\bar{\underline{m}}},$$

which we write, as in (39), as

$$\dot{\underline{x}} = \underline{f}(\underline{x}, \underline{p}), \text{ where } \underline{f} = \underline{\underline{Q}}_1^{-1} \cdot (\bar{\underline{m}} - \underline{\underline{Q}}_2 \underline{x})$$

and $\underline{p}$ is the column matrix of all system parameters.

As in section 7.2, we proceed to compute the reference solution $\underline{x}^*$ from $\underline{f}(\underline{x}^*, \underline{p}) = 0$. Since $\underline{f}$ is a nonlinear function, we can not expect to solve the equations of motion analytically for $\underline{x}^*$. But for a given parameter set $\underline{p} = \{\Omega, o, EI, \beta, \mu, \omega_0, M_\infty\}^T$, this can be done numerically. We set $\Omega = 20^o/\text{s}$, $M_0 = M_\infty(2 - o)$ with $o = 0.2$, $EI = 210 \cdot 10^3$ N m^2, $\beta = 10^{-4}$ s, $\omega_0 = 72^o/\text{s}$ and $M_\infty = 60$ Nm and find

$$\underline{x}^* = \begin{pmatrix} 0 \\ 0 \\ -0.0002 \\ +0.0001 \end{pmatrix},$$

which is $\dot{W}_0^* = 0$, $\dot{W}_\ell^* = 0$, $W_0^* = -0.0002$ and $W_\ell^* = 0.0001$. Linearization as in (41) about $\underline{x}^*$ and solving the eigenvalue-problem yields with $\jmath = \sqrt{-1}$

$$\lambda_{1/2} = -1.9\frac{1}{\text{s}} \pm \jmath\, 256\frac{1}{\text{s}}, \quad \lambda_{3/4} = 0.05\frac{1}{\text{s}} \pm \jmath\, 56\frac{1}{\text{s}}.$$

λ_3 and λ_4 have positive real parts, which means instability! This gives a red dot in the stability map. We repeat this procedure for all combinations (Ω, o) we are interested in and get the following stability map:

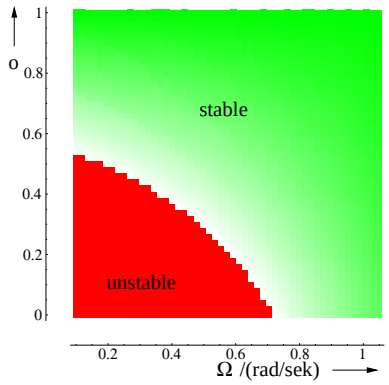

Figure 32: Stability of reference solution.
The more intense a green mark is, the smaller is the maximum real part of the respective eigenvalues. The number of (Ω, o)-combinations in this example is 50×50. Each combination is represented by one red or green rectangle.

8 Stability of airfoil-eigenmodes

We aim to reveal processes, which lead to instable wind turbine operation. Parameter-ranges where these instabilities occur must be found.

The authors opinion is, that instabilities of wind turbines can be related to two excitation mechanisms:

- **Parameter-Excitation:** Periodic coefficients in systems of differential equations – as for example in HAWC ([10], sec. E) – may produce instability. Mathieu's linear differential equation

  $$\ddot{x} + (\lambda + \gamma \cos(\Omega t))x = 0$$

  is a famous example. A more common example for parameter excitation is a bicycle with a bump in the front wheel. For certain speeds in free-hand-riding does the bump induce handlebar oscillations.
- **Self-Excitation** Self-excitation occurs in systems of nonlinear differential equations. The physical system steers the flow of energy, so that it self-sustains oscillations.

This section is dedicated to self-excitation. The reason for this choice is not, that parameter excitation seems less likely, but that we can hope to study self-excitation mechanisms on very simple subsystems of the turbine. We investigate the stability of an airfoil section, which is elastically supported in a wind tunnel.

Usually, a system as in Figure 33 is investigated.

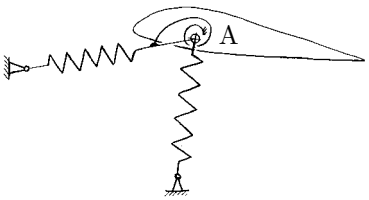

Figure 33: Airfoil-section with three degrees of freedom.

It has three degrees of freedom, which are only coupled by external (including inertia) forces. Thus, a vertical force applied in A results only in a vertical displacement, which is normally not the case.

We choose a different approach. Let's assume, the motions of an airfoil in self-excitation are similar to one of its eigenmodes. Then, horizontal and vertical displacements and rotation of an airfoil-section follow a prescribed coupling and can be described by only one time dependent amplitude function. This idea will be presented in the following.

8.1 Kinematics

For a real blade, we can find eigenfrequencies and eigenmodes for the whole airfoil from FEM-computations or measurements. For our model, we cut a short section of width ℓ_W out of the airfoil and adjust the beam springs in Figure 34, so that the airfoil-section oscillates with same frequency and displacement-modes as in a blade.

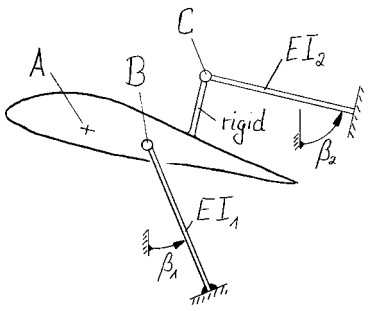

Figure 34: Our model of an airfoil-section with one degree of freedom.

We investigate the stability of this system in an 2D airflow, allowing only for motions in the cross-sectional plane.

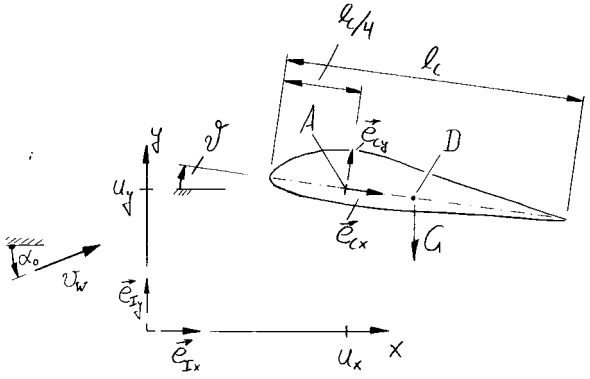

Figure 35: Coordinates and system parameters.

Point A is a reference point and lies on the cord (cord length ℓ_C) of the airfoil-section, $\ell_C/4$ from the leading edge. Let its position in x-y-coordinates in an inertial system be

$$\begin{aligned}\vec{r}_A &= u_x(t)\,\vec{e}_{Ix} + u_y(t)\,\vec{e}_{Iy} \\ &= \{u_x(t), u_y(t)\}\cdot\underline{\vec{e}}_I\end{aligned}$$

The cord-fixed coordinate-system $\underline{\vec{e}}_C = \{\vec{e}_{Cx}, \vec{e}_{Cx}\}^T$ has its origin in A and is related to $\underline{\vec{e}}_I$ by

$$\underline{\vec{e}}_C = \underbrace{\left\{\begin{array}{cc}\cos(\vartheta(t)) & -\sin(\vartheta(t)) \\ \sin(\vartheta(t)) & \cos(\vartheta(t))\end{array}\right\}}_{=:\,\underline{\underline{D}}(\vartheta(t))}\cdot\underline{\vec{e}}_I$$

and gives the position vectors of B, C and D (see Figures 34 and 35) to

$$\begin{aligned}\vec{r}_B &= \vec{r}_A + \{\ell_1, 0\}^T\cdot\underline{\vec{e}}_C\ , \\ \vec{r}_C &= \vec{r}_A + \{\ell_2,\ell_4\}^T\cdot\underline{\vec{e}}_C \text{ and} \\ \vec{r}_D &= \vec{r}_A + \{\ell_3, 0\}^T\cdot\underline{\vec{e}}_C\ .\end{aligned}$$

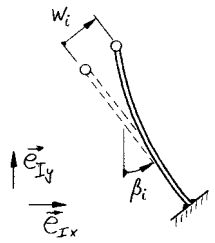

Figure 36: Beam-support of airfoil.

For small displacements, points B, C can only move perpendicular to the longitudinal blade axis, thus

$$\begin{aligned} \vec{r}_B &\stackrel{!}{=} \{w_1(t)\cos(\beta_1), w_1(t)\sin(\beta_1)\} \cdot \underline{\vec{e}}_I \text{ and} \\ \vec{r}_C &\stackrel{!}{=} \{w_2(t)\cos(\beta_2), w_2(t)\sin(\beta_2)\} \cdot \underline{\vec{e}}_I \end{aligned} \tag{45}$$

resulting in four algebraic constraints for the motion of the airfoil-section. With (45), we express u_x, u_y, ϑ and w_2 as functions of w_1. We are thus left with only one dependent coordinate for the airfoil section.

8.2 Equations of Motion

Airfoil-Section Motion

The kinetic energy of the airfoil-section is

$$T = \frac{1}{2} M \, \dot{\vec{r}}_D \cdot \dot{\vec{r}}_D + \frac{1}{2} J \dot{\vartheta}^2 \tag{46}$$

with M, J being mass and moment of inertia of the airfoil. Potential energy U is elastic energy stored in the deformed, massless beams (stiffness k_1, k_2) and force potential due to weight $G = Mg$:

$$U = \frac{1}{2} k_1 w_1(t)^2 + \frac{1}{2} k_2 w_2(t)^2 + G \, \vec{r}_D \cdot \vec{e}_{Iy} \; . \tag{47}$$

Virtual work $\tilde{\delta} W$ of non-potential forces comes from material damping in the beams (damping coefficient d) and aerodynamic forces $\vec{f}$ and moments m on the airfoil-section:

$$\tilde{\delta} W = -\frac{1}{2} d \left(k_1 \dot{w}_1(t) \; \tilde{\delta} w_1 + k_2 \dot{w}_2(t) \; \tilde{\delta} w_2 \right) + \vec{f}(t) \cdot \tilde{\delta} \vec{r}_A + m(t) \cdot \tilde{\delta} \vartheta \; . \tag{48}$$

Flow Description

Aerodynamic loads are superpositioned from one part, resulting from the generation of pressure waves (index W) and another one, originating from circulation (index γ). Thus $\vec{f} = \vec{f}_W + \vec{f}_\gamma$ and $m = m_W + m_\gamma$.

Generation of Pressure Waves

As described for example in [3] and [12], an oscillating airfoil dissipates mechanical energy in form of pressure waves.

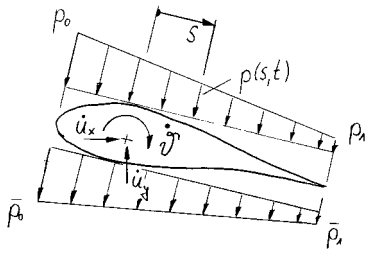

Figure 37: Generation of pressure-waves.

As the blade moves upwards, it generates a high pressure region on top of the blade (pressure coordinates $p_0(t)$, $p_1(t)$) and low pressure regions below (pressure coordinates $\bar{p}_0(t)$, $\bar{p}_1(t)$) – just as a loudspeaker does.

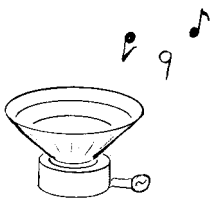

Figure 38: Analogy: loudspeaker.

For slow motions, no sound is emitted – just as with loudspeakers without chassis, because air-particles are transported from high to low pressure regions. This is called an acoustic short circuit. We find

$$\begin{aligned}
&p_0(t)=\varrho a\left(\frac{\mathrm{d}}{\mathrm{d}t}\left(\vec{r}_A+(-\ell_C/4,0)\cdot\underline{\vec{e}}_C\right)\right)\cdot\vec{e}_{Cy}-q_0(t)\ ,\\
&p_1(t)=\varrho a\left(\frac{\mathrm{d}}{\mathrm{d}t}\left(\vec{r}_A+(+3\ell_C/4,0)\cdot\underline{\vec{e}}_C\right)\right)\cdot\vec{e}_{Cy}-q_1(t)\ ,\\
&\bar{p}_0(t)=-p_0(t) \text{ and}\\
&\bar{p}_1(t)=-p_1(t)\ .
\end{aligned} \tag{49}$$

where $q_0(t)$, $q_1(t)$ describe mass transport due to acoustic short circuit and a is the speed of sound. Let the equations of motion for $q_0(t)$, $q_1(t)$ be

$$\dot{q}_0(t)=T_a\left(p_0(t)-\bar{p}_0(t)\right) \text{ and } \dot{q}_1(t)=T_a\left(p_1(t)-\bar{p}_1(t)\right) \tag{50}$$

with T_a being a time constant.

The resulting forces $\vec{f}_W=\underline{f}_{C,W}\vec{\underline{e}}_C=\underline{f}_{I,W}\vec{\underline{e}}_I$ and moment m_W per unit airfoil width are obtained by integrating $p(s,t)=(1-(s+1/4))\cdot p_0(t)-(s+1/4)\cdot p_1(t)$ over cord length ℓ_C:

$$\begin{aligned}
f_{Cy,W} &= \int_{-\frac{\ell_C}{4}}^{\frac{3\ell_C}{4}} -2\,p(s,t)\mathrm{d}s\ ,\\
f_{Cx,W} &:= 0 \qquad\qquad \text{and}\\
m_W &= \int_{-\frac{\ell_C}{4}}^{\frac{3\ell_C}{4}} +2\,s\,p(s,t)\mathrm{d}s\ .
\end{aligned}$$

We relate aerodynamic lift and moment to two flow characteristics, describing aerodynamic circulation around the airfoil and flow detachment. Let γ be proportional to circulation and δ be the normalized point of flow detachment measured from the trailing edge. Lift coefficient C_L is defined as $C_L = a_L\ \gamma$ with constant a_L.

Equations of motion for γ and δ read

$$\begin{aligned} T_\gamma \dot{\gamma} + \gamma &= s(p_3 \Delta\gamma) \cdot \exp p_2 \delta \\ T_\delta \dot{\delta} &= \left(\Delta\gamma - \frac{\alpha(t)}{\alpha_\delta (1 + \frac{1}{2}\frac{p_3}{p_1})} - p_5 \delta \right) \cdot \exp -p_4 \dot{\gamma} \ . \end{aligned} \tag{51}$$

with $\Delta\gamma := \frac{\alpha(t)}{\alpha_\delta} - \gamma(t)$, parameters p_i and degressive function $s(\zeta)$:

$$s(\zeta) = \begin{cases} \dfrac{\sqrt{\zeta^2 + 1} - 1}{\zeta} & \text{for } \zeta \neq 0 \\ 0 & \text{for } \zeta = 0 \end{cases} \quad .$$

Function s accounts for the viscosity driven force, which attaches the flow to the airfoil. Parameters T_γ, T_δ, p_1, p_2, p_3, p_4 and p_5 are unknown. From lift measurements under stationary conditions [7], we identify p_1, p_2, p_3, p_5 and a_L.

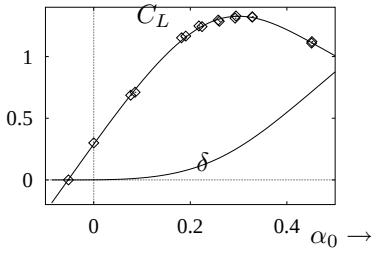

Figure 39: Characteristic curve C_L for system parameters identified from [7] (dots) and computed δ.

T_γ, T_δ and p_4 are chosen appropriately.

Lift $f_{\gamma L}$, drag $f_{\gamma D}$ and moment m_γ per unit blade width are

$$\begin{aligned} f_{\gamma L} &= \tfrac{\varrho}{2} \bar{v}_{rel}^2 C_L(\gamma)\ \ell_C \ , \\ f_{\gamma D} &= \tfrac{\varrho}{2} \bar{v}_{rel}^2 C_D(\gamma, \delta)\ \ell_C \ , \\ m_\gamma &= \tfrac{\varrho}{2} \bar{v}_{rel}^2 C_M(\gamma, \delta)\ \ell_C^2 \ . \end{aligned}$$

The contribution $\vec{f}_\gamma$ to the force vector $\vec{f}$ from (48) is then

$$\vec{f}_\gamma = \{f_{\gamma D}, f_{\gamma L}\} \cdot \underline{\underline{D}}(-\alpha(t)) \cdot \underline{\vec{e}}_I$$

with $\alpha(t)$ being the angle of attack. It depends on α_0, the angle of attack under stationary conditions and the motion of the airfoil. We compute $\alpha(t)$ from the flow velocity of point A relative to the flow far enough from the airfoil:

$$\vec{v}_{rel} = \{v_W, 0\} \cdot \underline{\underline{D}}(-\alpha_0) \cdot \underline{\vec{e}}_I - \dot{\vec{r}}_A$$

resulting in

$$\tan(\alpha(t)) = \frac{v_{rel,y}}{v_{rel,x}} \text{ and } \bar{v}_{rel}^2 = v_{rel,x}^2 + v_{rel,y}^2.$$

System of Differential Equations

From the principle of Hamilton-Ostrogradskij we obtain one ordinary, nonlinear differential equation of second order for the airfoil-section:

$$m\,\ddot{w}_1 + b\,\dot{w}_1 + k\,w_1 = f(w_1, \dot{w}_1, q_0, q_1, \gamma, \delta)\ . \tag{52}$$

Four nonlinear differential equations of first order describe the airflow (see equations (50), (51)):

$$\begin{aligned}
\dot{q}_0(t) &= T_a\,(p_0(t) - \bar{p}_0(t))\ , \\
\dot{q}_1(t) &= T_a\,(p_1(t) - \bar{p}_1(t))\ , \\
T_\gamma\dot{\gamma} + \gamma &= s(p_3\Delta\gamma)\cdot\exp p_2\delta \qquad \text{and} \\
T_\delta\dot{\delta} &= \left(\Delta\gamma - \frac{\alpha(t)}{\alpha_\delta(1 + \frac{1}{2}\frac{p_3}{p_1})} - p_5\delta\right)\cdot\exp -p_4\dot{\gamma}\ .
\end{aligned}$$

Defining $\dot{w}_1 \equiv v_1$, we write the above equations with $\underline{x} = \{v_1, w_1, q_0, q_1, \gamma, \delta\}^T$ as

$$\dot{\underline{x}} = \underline{f}(\underline{x}, \underline{p})\ ,$$

with $\underline{p}$ being the column matrix of all system parameters.

8.3 Linear Stability Analysis

A stationary solution $\underline{x}^*$ of our system fulfills $\dot{\underline{x}} \equiv 0$, giving a nonlinear system of equations for $\underline{x}^*$:

$$\underline{0} = \underline{f}(\underline{x}^*, \underline{p})\ .$$

We decide about the stability of $\underline{x}^*$ by allowing small oscillations $\underline{\zeta}(t)$ about $\underline{x}^*$: $\underline{x}(t) = \underline{x}^* + \underline{\zeta}(t)$ and solve the linearized equations of motion as eigenvalue problem associated with

$$\dot{\underline{\zeta}}(t) + \underline{\underline{A}}\cdot\underline{\zeta}(t) = \underline{0}$$

where the matrix elements $a_{i,j}$ of $\underline{\underline{A}}$ are

$$a_{i,j} = \left.\frac{\partial f_i}{\partial x_j}\right|_{\underline{x}(t) = \underline{x}^*}\ .$$

The following numerical results are chosen to match the lift-drag-characteristic identified from [7]. The parameters for the time (T_a, T_δ, T_γ) constants in the model are chosen as appropriate as possible.

Parameters are listed in section 8.3 unless otherwise specified in the description of the figures.

Green areas mean stability, red instability with colour-intensity relating to the degree of stability.

Blue areas indicate, that the numerical root finding routine to compute the stationary solution failed. This could indicate, that no stationary solution exists in the valid range of the state variables or simply, that the root finding procedure was not successful.

"Full" intensity corresponds to damping ratio = ± 1 (damping ratio = viscous damping factor), where no oscillations are possible - the solution grows or decreases in form of an exponential function.

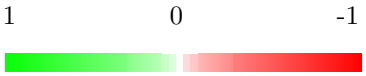

Figure 40: Colour intensity related to damping ratio.

As a reference case, stability maps for $\beta_1 \equiv \beta_2$ (no pitching of the airfoil) are computed for different values of T_γ. Angle of attack α ranges from 0 grad $\leq \alpha \leq$ 25 grad, β_1 (and thus β_2) goes from 0 grad $\leq \beta \leq$ 100 grad, thus covering the range from flapwise to edgewise vibrations.

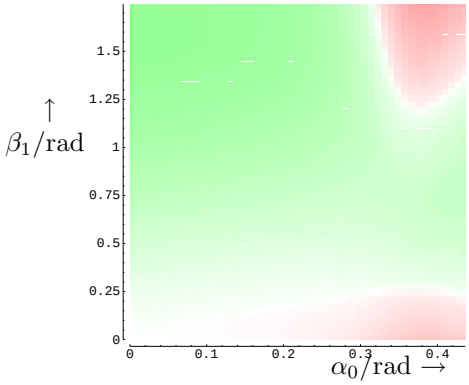

Figure 41: Stability map, $\beta_2 = \beta_1$, $T_\gamma = 0.0001$.

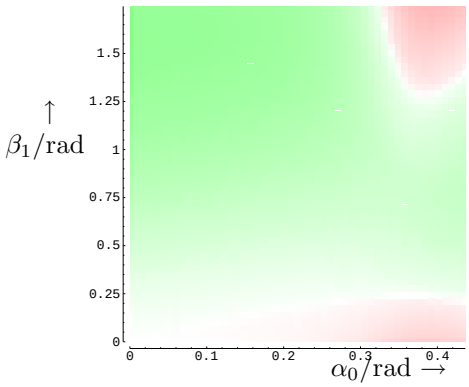

Figure 42: Stability map, $\beta_2 = \beta_1$, $T_\gamma = 0.001$.

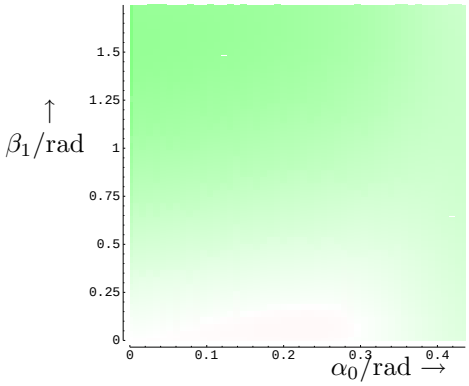

Figure 43: Stability map, $\beta_2 = \beta_1$, $T_\gamma = 0.01$.

In the following, we give few results from stability investigations without further comments.

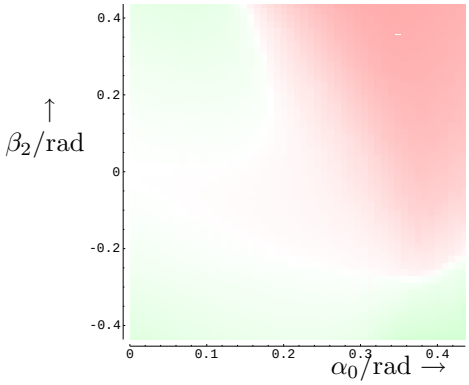

Figure 44: Stability map, $\beta_1 = 0$, $T_\gamma = 0.0001$.

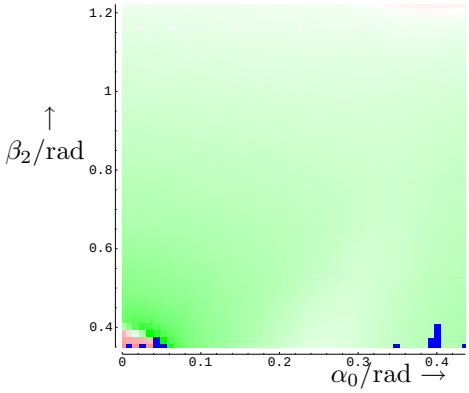

Figure 45: Stability map, $\beta_1 = 45$ grad, $T_\gamma = 0.0001$.

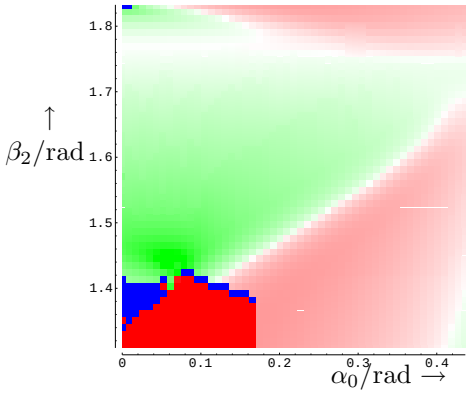

Figure 46: Stability map, $\beta_1 = 90$ grad, $T_\gamma = 0.0001$.

Conclusion and Forward Look

Linear stability analysis is a very effective approach to determine upon stability of our system. Cumbersome numerical integration of the nonlinear system is not necessary and numerically generated instabilities can be precluded. Wide parameter ranges can systematically be searched for parameter-combinations that produce instability and very comprehensive results are obtained.

A disadvantage of our approach is, that we are limited to small oscillations around a stationary solution. Thus, instability might occur even in parameter ranges that were predicted to be stable with linear stability analysis.

The results given must be seen as purely experimental, because

- the aerodynamic model has only been validated for stationary flow,
- the functional relation between C_D, C_M and γ, δ has been chosen with some arbitrariness, and
- the question remains, if our assumption, that the blade oscillates self-excitedly in one of its eigenmodes, holds.

System Parameters

parameter	value
α_0	20^o
α_δ	10^o
v_W	20 m/s
ℓ_C	1 m
T_δ	$10 \cdot T_\gamma$
p_1	0.4
p_2	1.3
p_3	1.0
p_4	0.0 s
p_5	1.0
p_6	0.0
p_7	10.0
a_L	1.6
$a_{D,0}$	0.1
$a_{D,1}$	0.6
$a_{D,2}$	0.7
$a_{M,0}$	-0.05
$a_{M,1}$	-0.1
$a_{M,2}$	-0.08
a	331 m/s
ϱ	1.225 kg/m^3
T_a	0.0001 s
M	10 kg
J	0.1 kg m^2
k_1	1000 N/m
k_2	1000 N/m
d	0.0001 s
ℓ_1	0.2 m
ℓ_2	0.5 m
ℓ_4	0.1 m
ℓ_3	0.1 m
g	9.81 m/s^2
ℓ_W	1 m

8.4 Model Extension to Three Independent Degrees of Freedom for the Cross Section

So far, the dynamic instabilities described are only special cases, because only one structural degree of freedom is accounted for. We extend the model to allow for free inplane motions of the cross section. The coordinates of the quarter-cord point are flapwise and edgewise deflection and cross section rotation.

It is inconvenient to derive the equations of motion for the cross section using spring arrangements in order to achieve a certain desired dynamical behaviour. Instead of, we solve the inverse problem: We define the system dynamics in form of eigenfrequencies and eigenvectors and compute the system matrices.

The definition file for the eigensystem of the cross section looks like this:

```
(*
    Defines the Eigenmodes for the cross section
    giving Eigenfrequency and Eigenvector

    Note: The Eigenvector do not have to be orthogonal:
      An orthogonal approximation of the EV is computed automatically

*)

eigensystem = {{2.7  Hz, {1.00 meter,-0.25  meter, 0.010 }},
       {1.3  Hz, {0.25 meter, 1.000 meter,-0.010 }},
       {20.7 Hz, {0.05 meter,-0.12  meter, 1.000}}}
```

For the given "eigenvectors", a Mathematica Program computes an approximation where the eigenvectors are orthogonal. A mass per unit blade length and a moment of inertia per unit blade length must be prescribed. Then the equations of motion for the cross section can be derived.

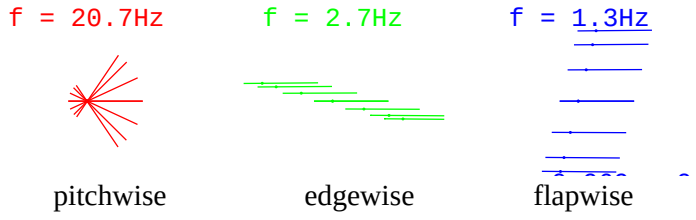

Figure 47: Eigenmodes approximated by Mathematica.

The equations of motion for the aerodynamic loads is the same as described in the preceding section. Also, the linear stability analysis is performed as described above.

The example given below shows the importance of the time constants T_γ (T_δ) for the aeroelastic stability of the system.

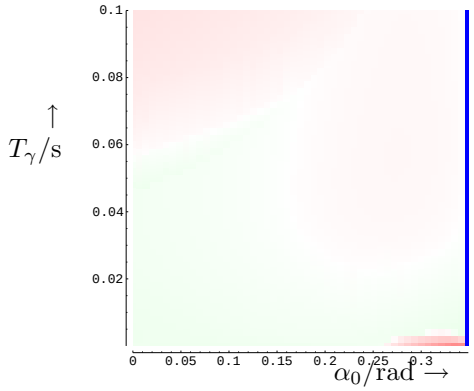

Figure 48: Stability map, $T_\delta = 5T_\gamma$ (see (51)).

Suggestions for Further Work

The mathematical model for the flow description has the major advantage to introduce state variables related to aerodynamic lift, drag and moment. This allows a very systematic stability analysis – as seen above. But further application of the model is only useful, if it can be validated, and its system parameters can be identified from measurements.

9 Self Excitation of Wind Turbine Blades

A mathematical model for one wind turbine blade rotating around a spatially fixed axis and for the aerodynamic loads on the blade is derived.
The blade model uses a subdivision of the structure into small elements as in the method of Finite Elements, but form-functions for flexure, torsion, extension, shear and warping are global (stretching over the whole blade length). The coordinates describing extension, shear and warping can be eliminated without neglecting the important elastic coupling between flexure and torsion.
Aerodynamic loading of the blade is described by introducing first order differential equations for circulation γ and flow detachment δ. C_L, C_D and C_M are simple functions of γ and δ. Based on a wave type solution, the emission of acoustic waves by the blade, and thus the dissipation of mechanical energy, is accounted for.
A systematic linear stability analysis is carried out, and bounds for stable operation are found.

9.1 Introduction

Flutter can be an essential design limitation for elastic structures interacting with fluid flow. Self excitation of aircrafts due to coupling of elastic wings and air flow has been studied intensively, but little is known about aeroelastic instability of wind turbines.

First, a blade model describing the structural dynamics must be derived. We are interested in flexural and torsional motions of the blade and especially in an elastic coupling of these deformations.

Second, an aerodynamic model must be stated to describe air loads on the blade.

In order to perform a systematic stability analysis, the mathematical model must be expressible as a system of ordinary differential equations with state variables $\underline{Y}$ as $\dot{\underline{Y}} = \underline{f}(\underline{Y})$ and the number of the differential equations shall be moderately small (say order < 100). Large FE models for blade or airflow are therefore unacceptable. In the following, we will present a Galerkin type blade model and a phenomenological dynamic stall model derived from Leishman and Beddoes (1986).

In order to simplify the stability analysis and to avoid periodic coefficients in the differential equations, which could be another source of dynamic instability, we investigate the simplified model from Figure 49. One blade of viscoelastic, isotropic material rotates around a spatially fixed axis.

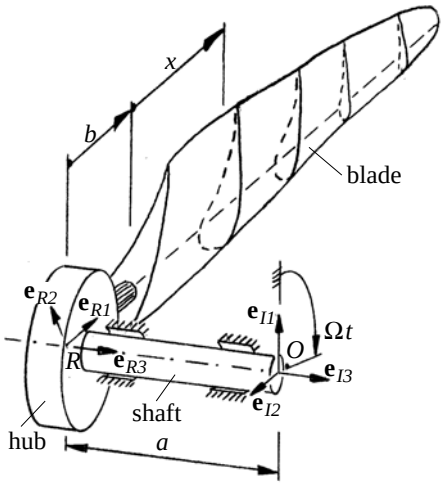

Figure 49: Sketch of wind turbine blade rotating about a spatially fixed axis.

In the modeling process, we will first define coordinates describing the motion of the blade as in the theory of rods (Antmann, 1995). Then the stiffness matrix will be derived and the coordinates for extension, tilt and warping of the cross sections will be eliminated from the system of differential equations.

From the virtual work of d'Alembert forces, the mass matrix and gyroscopic terms due to rotation with Ω will be derived. Then differential equations for circulation and detachment of the flow will be chosen and discretized with Finite Elements. The linear stability analysis finds stationary solutions of the system of differential equations and decides upon their stability. Parameter studies show stability bounds for the blade operation.

9.2 Kinetics

We denote a vector in 3D space by a lower-case, boldface symbol, ($\underline{.}$) denotes a column matrix and ($\underline{\underline{.}}$) a matrix.

A Cartesian coordinate system with origin O in one end of the rotor shaft is spanned by the unit vectors $\{\mathbf{e}_{I1}, \mathbf{e}_{I2}, \mathbf{e}_{I3}\}^T =: \underline{\mathbf{e}}_I$ with $\mathbf{e}_{I3}$ parallel to the shaft axis. In O the shaft is rotated with constant angular velocity Ω. The other end of the twistable shaft is connected to hub and blade of length ℓ. The blades reference axis A is perpendicular to $\mathbf{e}_{I3}$. The distance from rotor center R to the blade root is b, the longitudinal coordinate from the bladeroot along A be x.

We define the blade geometry by N profiles at $x = x_n$, $n = \{1, \ldots, N\}$. Profile P_n at x_n is a polygon and we generate a cross section by computing a polygon with constant offset to P_n and by eliminating intersections (see Figure 50). Thus each cross section is defined by tetragons. Connecting the corner points of two tetragons on neighboring cross sections by lines defines a polyeder. Those are the volume elements, the blade is made of.

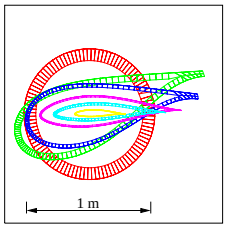

Figure 50: Definition of cross sections.

In the strainless reference configuration, a point $\{x, y, z\}$ of the blade is identified by the local reference vector

$$\mathbf{r}^{ref} = \mathbf{r}_R + \{b + x, y, z\}^T \cdot \underline{\mathbf{e}}_R,$$

where $\mathbf{r}_R = \{0, 0, a\}^T \cdot \underline{\mathbf{e}}_I$ is the vector from O to the rotor center R, $\underline{\mathbf{e}}_R$ is the column matrix of the unit vectors in the rotor coordinate system and $\{x, y, z\}$ are coordinates of the blade material in the $\underline{\mathbf{e}}_R$ system. Transformation from $\underline{\mathbf{e}}_I$ into $\underline{\mathbf{e}}_R$ is a rotation $\underline{\underline{R}}_3$ about the "3"-axis as $\underline{\mathbf{e}}_R = \underline{\underline{R}}_3(-\Omega t)\ \underline{\mathbf{e}}_R$ with matrix

$$\underline{\underline{R}}_3(.) := \begin{pmatrix} \cos(.) & \sin(.) & 0 \\ -\sin(.) & \cos(.) & 0 \\ 0 & 0 & 1 \end{pmatrix}.$$

The position of point $\{x, y, z\}$ for deformed shaft and blade be

$$\begin{aligned} \mathbf{r} = \quad & \mathbf{r}_R + \\ & \{b + x + u_1(x,t), u_2(x,t), u_3(x,t)\}^T \cdot \underline{\underline{R}}_3(-\Omega t + \Theta(t))\underline{\mathbf{e}}_I + \\ & \{\sum_{i=1}^{I} \Upsilon_i(y,z) \cdot \psi_i(x,t), y, z\}^T \cdot \\ & \underline{\underline{R}}_1(\varphi_1(x,t))\underline{\underline{R}}_2(\varphi_2(x,t))\underline{\underline{R}}_3(\varphi_3(x,t))\underline{\underline{R}}_3(-\Omega t + \Theta(t))\underline{\mathbf{e}}_I \end{aligned} \tag{53}$$

with $\underline{\underline{R}}_1$, $\underline{\underline{R}}_2$ being the rotational tranformations about the respective 1 and 2-axis. Angle $\Theta(t)$ describes a twist of the shaft, u_1, u_2, u_3 are deflections of cross section x, angles φ_1, φ_2, φ_3 are rotation and tilt angles and ψ_i, $i = 1, \ldots, 3$ are out of plane deformations (warping) of the cross section. We choose $I = 3$ and $\Upsilon_1 = yz$, $\Upsilon_2 = y^2$ and $\Upsilon_3 = z^2$.

Linearization with respect to all dependent coordinates yields

$$\begin{aligned} \mathbf{r}^{lin} = \quad & (b + x + u_1 - y \cdot \varphi_3 + z \cdot \varphi_2 + yz \cdot \psi_1 + y^2 \cdot \psi_2 + z^2 \cdot \psi_3)\ \mathbf{e}_{R1} + \\ & (y + u_2 - z \cdot \varphi_1)\ \mathbf{e}_{R2} + \\ & (z + u_3 + y \cdot \varphi_1)\ \mathbf{e}_{R3}\ . \end{aligned} \tag{54}$$

Note that the warping functions ψ_i can be interpreted as part of a Taylor series of the deflection in x-direction to second order in y and z.

9.3 Equations of Motion

The principle of virtual work states that

$$\begin{aligned} \delta W := \quad & \delta W_E + \delta W_V + \delta W_A + \delta W_D \\ \stackrel{!}{=} \quad & 0, \end{aligned}$$

where δW_E is the virtual strain energy, δW_V is the virtual work of volume forces (here only d'Alembert forces), δW_A is the virtual work of aerodynamic forces and δW_D is the virtual work of viscous damping of the structure. We shall introduce form-functions used to discretize the blade motion and integrate numerically over each polyeder.

We abbreviate $\dot{(.)} = \partial(d)(.)/\partial t$ and $(.)' = \partial(d)(.)/\partial x$.

9.4 Stiffness Matrix

From Washizu (1982) we obtain

$$\delta W_E = \sum_{m=1}^{M} \int_{V_m} \sigma_{ij}\ \delta\varepsilon_{ij} \mathrm{d}V + K\Theta\ \delta\Theta \tag{55}$$

where V_m is the volume of polyeder m, M is the number of polyeders the blade consists of, σ_{ij} is a component of the stress tensor, ε_{ij} is a component of the linearized Green strain tensor, δ is the variation sign and K is the torsional stiffness of the blade shaft.

For a slender rod as the blade, we may assume that $\sigma_{yy} \equiv 0$, $\sigma_{zz} \equiv 0$. From the stress-strain-relations (Hook's law), we obtain with modulus of elasticity E and modulus of shear G

$$\sigma_{xx} = E\varepsilon_{xx}\ , \sigma_{xy} = 2G\varepsilon_{xy}\ , \sigma_{xz} = 2G\varepsilon_{xz}\ , \sigma_{yz} = 2G\varepsilon_{yz}\ ,$$
$$\varepsilon_{yy} = (1 - \frac{E}{2G})\varepsilon_{xx}\ , \varepsilon_{zz} = (1 - \frac{E}{2G})\varepsilon_{xx}\ .$$

Deflections u_i, φ_i, ψ_i are discretized using

$$u_i(x,t) = \sum_{j=1}^{N(ui)} U_{ij}(t) \left(\frac{x}{\ell}\right)^j\ ,\quad \varphi_i(x,t) = \sum_{j=1}^{N(\varphi i)} \Phi_{ij}(t) \left(\frac{x}{\ell}\right)^j\ ,$$
$$\psi_i(x,t) = \sum_{j=1}^{N(\psi i)} \Psi_{ij}(t) \left(\frac{x}{\ell}\right)^j\ . \tag{56}$$

The integral over the blade volume in equation (55) is solved numerically. Let $\underline{Z} = (\Theta, U_{21}, \ldots, U_{2N(u2)}, U_{31}, \ldots, U_{3N(u3)}, \Phi_{11}, \ldots, \Phi^T_{1N(\varphi 1)})$ and $\underline{Q} = (U_{11}, \ldots, U_{1N(u1)}, \Phi_{21}, \ldots, \Phi_{3N(\varphi 3)}, \Psi_{11}, \ldots, \Psi_{3N(\psi 3)})^T$. $\underline{Z}$ holds the dependent coordinates, which are essential to the description of the blades flexure and torsion, $\underline{Q}$ holds the remaining coordinates that dominate high-frequency solutions, which we are not interested in. They contribute to flexure and torsion by a kind of forced sverwing motion.

The differential equations in $\underline{Z}$ and $\underline{Q}$ are

$$\begin{pmatrix} \underline{\underline{K}}_{ZZ} & \underline{\underline{K}}_{ZQ} \\ \underline{\underline{K}}_{QZ} & \underline{\underline{K}}_{QQ} \end{pmatrix} \begin{pmatrix} \underline{Z} \\ \underline{Q} \end{pmatrix} = \begin{pmatrix} \underline{f}_Z \\ \underline{f}_Q \end{pmatrix} \tag{57}$$

with $\underline{f}_Z$, $\underline{f}_Q$ resulting from δW_V, δW_D and δW_A. In equation (57), we neglect the parts of virtual works in $\delta\underline{Q}$ other than δW_E, thus declaring $\underline{f}_Q = \underline{0}$. This

simplification is justified, because we may assume that airloads do not depend explicitly on $\underline{Q}$ and that the d'Alembert forces related to $\underline{Q}$ do not contribute significantly to the motion of interest. Thus, deformations $\underline{Q}$ are slaved to the coordinates $\underline{Z}$ (and δQ vanishes)! Then equation (57) reads $\underline{\underline{K}}_{ZZ}\underline{Z}+\underline{\underline{K}}_{ZQ}\underline{Q}=\underline{f}_Z$ with $\underline{Q}=-\underline{\underline{K}}_{QZ}^{-1}\underline{\underline{K}}_{QQ}\underline{Z}$ and we obtain

$$\delta W_E = \delta\underline{Z}^T \underbrace{\left(\underline{\underline{K}}_{ZZ} - \underline{\underline{K}}_{ZQ}\underline{\underline{K}}_{QZ}^{-1}\underline{\underline{K}}_{QQ}\right)}_{=:\,\underline{\underline{K}}^*} \underline{Z}\,.$$

For simplicity, we introduce (proportional) damping as

$$\delta W_D = \delta\underline{Z}\,(\beta\underline{\underline{K}}^*)\,\dot{\underline{Z}}\,,$$

with damping coefficient β.

9.5 Matrices Resulting from d'Alembert Forces

The virtual work of d'Alembert forces is

$$\delta W_V = \sum_{m=1}^{M}\int_{V_m} \varrho_B \ddot{\mathbf{r}}^* \cdot \delta\mathbf{r}^* \mathrm{d}V + J\ddot{\Theta}\,\delta\Theta\,, \tag{58}$$

where $\mathbf{r}^* = \mathbf{r}\,|_{u_1=\tilde{u}_1,\varphi_{2,3}=0,\psi_i=0,i=1,..,3}$, ϱ_B is the blade density and J is the moment of inertia of the hub. Note that in equation (58), $\mathbf{r}^*$ must not be linearized. $\tilde{u}_1$ has a particular importance, because it is responsible for the gyroscopic terms in the differential equations. We compute $\tilde{u}_1$ under the assumption, that the blades reference axis x is inextensible:

$$\left(\frac{\partial\mathbf{r}^*}{\partial x}\right)\cdot\left(\frac{\partial\mathbf{r}^*}{\partial x}\right)\Bigg|_{(y=0,\,z=0)} \stackrel{!}{=} 1.$$

Solving this for $\tilde{u}_1'$ and developing it into a Taylor series until second order, we get $\tilde{u}_1(x,t) = \int_0^x(-u_2'(\xi,t)^2 - u_3'(\xi,t)^2)/2\,\mathrm{d}\xi$ (Bremer, 1988). The form-functions from equation (56) are introduced and integration over the blade yields

$$\delta W_V = \delta\underline{Z}^T\left(\underline{\underline{M}}_2\ddot{\underline{Z}} + \Omega\underline{\underline{M}}_1\dot{\underline{Z}} + \Omega^2\underline{\underline{M}}_0\underline{Z}\right)\,.$$

9.6 Aerodynamic Loads

Our idea is to compose simple equations of motion for state variables, which we relate to the lift $l(x,t)$, drag $d(x,t)$ and moment $m(x,t)$ per unit blade length that an airflow induces on a profile x of the blade.

Let $\mathbf{f}_A(x,t)$ be the aerodynamic force per unit blade length on the quarter cord point of the blade and $m(x,t)$ be the respective aerodynamic moment about the

$\mathbf{e}_{R3}$-axis. For simplicity, the blades reference (x-) axis is taken to be the connection of all quarter cord points of the profiles, thus

$$\delta W_A = \int_0^\ell \mathbf{f}_A \cdot \delta \mathbf{r}^* \big|_{(y=0,z=0)} + m \cdot \delta\varphi_1 \mathrm{d}x \ .$$

Note that the virtual rotation belonging to m is only so simple for this particular system setup. We built a dynamic stall model on the ideas of Leishman and Beddows (1986): The airloads $\underline{F}_A := (l, d, m)^T$ are separated into two parts $\underline{F}_A = \underline{F}_{A\gamma} + \underline{F}_{Aw}$, where index γ stands for airloads related to circulation of the air around the profile, and index w is associated with dissipation of compression waves off the blades surface.

Our justification for this separation assumption is that γ - associated with the generation of an ordered flow field - is a slow process (belonging to a slow time scale), while wave dissipation is assumed to be "fast". The coefficients of force $\mathbf{f}_A$ in the R-coordinate system are related by a rotation of angle of attack α to $\underline{F}_A$.

We define $\underline{F}_A = (C_l, C_d, C_m)^T \varrho_A/2 \cdot v^2 \ \ell_C$ with density of air ϱ_A, cord length $\ell_C(x)$, flow velocity relative to the profile $v(x,t)$ and a new set of functions C_l, C_d, C_m, which depend on the aerodynamic state variables, that we define in the following:

Let γ be proportional to flow circulation, thus defining $C_l(x,t) := C_{l1}\gamma(x,t)$ with parameter C_{l1} and let $\delta(x,t)$ be an indication for flow detachment. C_d and C_m must now be chosen as functions of γ and δ. In this work, we choose $C_D(x,t) = C_{d0} + C_{d1}\delta^2(x,t)$ and $C_M(x,t) = C_{m0} + C_{m1}\delta(x,t) + C_{m2}\delta^3(x,t)$. The equations of motion for γ and δ are functions of α. The scalar $v(x,t)$ is the absolute value of the projection of the flow velocity $\mathbf{v}_{A,rel}$ onto the cross sectional plane. With wind velocity v_W we compute $\mathbf{v}_{A,rel} = \dot{\mathbf{r}}^* - (0, 0, -v_W)^T \cdot \underline{\mathbf{e}}_I$. Angle of attack α is computed from the components of $\mathbf{v}_{A,rel}$ in cross sectional coordinates.

We choose two first order differential equations

$$\begin{aligned} T_\gamma \dot{\gamma} &= s(p_1 \Delta\gamma)\mathrm{E}^{p_2\delta} - \gamma \ , \\ T_\delta \dot{\delta} &= \Delta\gamma - \frac{\alpha - \alpha_0}{p_3\alpha_1} - p_4\delta \end{aligned} \tag{59}$$

with the digressive function $s(\zeta) = (\sqrt{\zeta^2 + 1} - 1)/\zeta$, abbreviations $\Delta\gamma = (\alpha - \alpha_0)/\alpha_1 - \gamma$ and parameters $p_1, \ldots, p_4$, α_0, α_1. δ is a phenomenological state variable, which can not be measured or defined in physical terms (such as eddy intensity). It is interpreted as a "hidden" state of the system. The differential equations are an appropriate model for *light stall with trailing edge separation*. The system parameters are identified from measurements (see Figure 51).

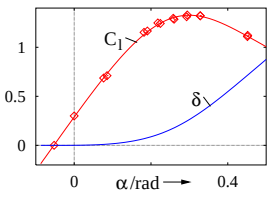

Figure 51: Characteristic curves C_L, δ for system parameters identified from [7] ($\diamond$).

Firgure 52 shows measured values for C_l, C_d and C_m and the equivalent model functions identified.

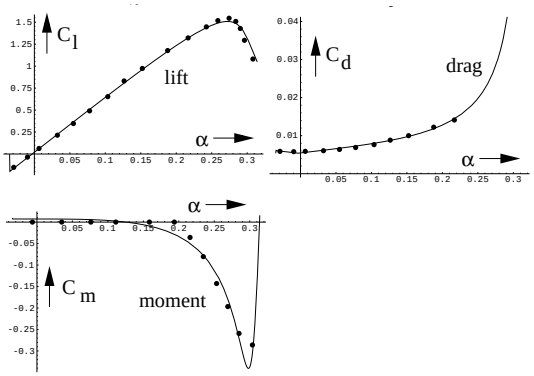

Figure 52: Comparison of measurements and fitted model. Results shown are for a NACA 0015 profile

Using Galerkins method (Fletcher, 1982), $\gamma(x,t)$ and $\delta(x,t)$ are discretized with piecewise linear form-functions along the blade length having N_A node variables $\Gamma_n(t)$ and $\Delta_n(t)$ each. Boundary conditions are $\gamma(\ell,t)=0$ and $\delta(\ell,t)=0$.

The contribution $\underline{F}_{Aw}$ of the airloads resulting from emission of compression waves is derived from a wave type-solution assuming one-dimmensional waves (Crighton et al., 1992). Here the blade is being thought as a flat plate of cord length $\ell_C(x)$ and length ℓ (see Figure 53).

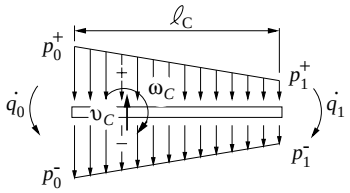

Figure 53: Pressure on blade due to wave dissipation. A linear pressure distribution along the cord length is assumed.

With velocity $v_C = v_C(x,\dot{\underline{Z}})$ and angular velocity $\omega_C = \omega_C(x,\dot{\underline{Z}})$ of the quarter cord point and speed of sound c_A, we find

$$\begin{aligned} p_0^+ &= \frac{1}{c_A}(v_C + \frac{\ell_c}{4}\omega_C) \; - q_0 = p_0^- \\ p_1^+ &= \frac{1}{c_A}(v_C - \frac{3\ell_c}{4}\omega_C) - q_1 = p_1^- \end{aligned}$$

where we subtracted q_0 and q_1 to account for an acoustic short circuit from high to low pressure regions on opposite sides of the blade. For q_0 and q_1 we choose the differential equations

$$\begin{aligned} T_q\dot{q}_0(x,t) &= p_0^+(x,t) - (-p_0^-(x,t)) \; , \\ T_q\dot{q}_1(x,t) &= p_1^+(x,t) - (-p_1^-(x,t)) \end{aligned} \tag{60}$$

which are discretized using piecewise linear form-functions as for γ and δ. The node variables Γ_i, Δ_i, Q_{0i} and Q_{1i} are collected in the column matrix of aerodynamic state variables $\underline{A}$.

The equations of motion of the aerodynamic model can now be solved in the time domain and the time dependent values of C_l, C_d, and C_m can be computed (Figure 54).

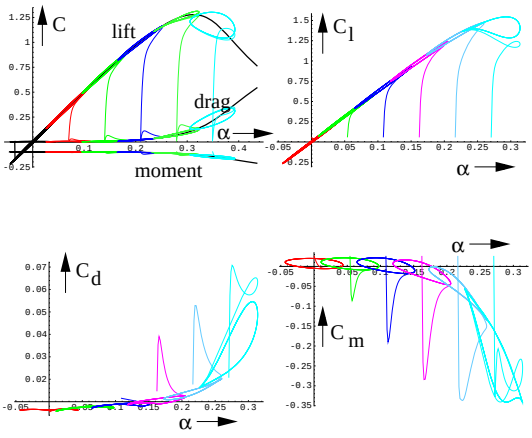

Figure 54: Integration of the equations of motion for γ and δ for $\alpha = \alpha_0 + 2.5\text{grad}\cos(\omega t)$.

By changing the values of T_q, T_δ and T_γ, the hysteresis loops can be widened and the direction of their principal axes with respect to the curve for the stationary aerodynamics can be influenced.

9.7 Linear Stability Analysis

The system of differential equations can now be written as

$$\underbrace{\begin{pmatrix} \ddot{\underline{Z}} \\ \dot{\underline{Z}} \\ \dot{\underline{A}} \end{pmatrix}}_{=:\dot{\underline{Y}}} = \underline{f}(\underline{Y}) \; . \tag{61}$$

It is composed of $1+N(u_2)+N(u_3)+N(\varphi_1)$ differential equations of second order for Θ, u_2, u_3, φ_1 and $4N_A$ differential equations of first order for γ, δ, p_0 and p_1. We choose $N(u_2) = 3$, $N(u_3) = 3$, $N(\varphi_1) = 3$ and $N_A = 8$, thus the overall order of equation (61) is 52. Unfortunately, the nonlinear right-hand side $\underline{f}$ can not be given in closed form due to the non-linearities associated with the computation of angle of attack α and flow velocity v. Therefore $\underline{f}$ has to be integrated numerically for each new $\dot{\underline{Z}}$, $\underline{Z}$ and $\underline{A}$. For $\ell = 19m$, a linear stability analysis finds stationary solutions $\underline{f}(\underline{Y}_0) = \underline{0}$ and investigates the stability of small oscillations around $\underline{Y}_0$. Figure 55 shows results of a parameter study for the wind speed v_W with $0\text{m/s} < v_W < 20\text{m/s}$ and the transition of an eigenvalue from instable to stable motion.

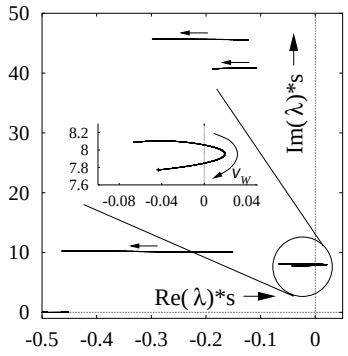

Figure 55: Path of eigenvalues λ in the complex plane as the wind speed v_W is increased. Arrows indicate orientation with increasing v_W.

The real part of the critical eigenvalue ($Re(\lambda)$) is plotted against the wind speed v_W in Figure 56.

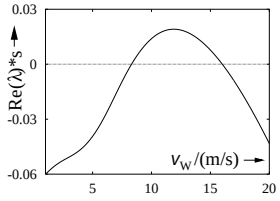

Figure 56: Real part of critical eigenvalue as function of wind speed v_W

The parameter space where instability occurs depends essentially on the time constants T_γ and T_δ. The instability shown is dominated by a flapwise motion and limit cycle oscillations can be found.

9.8 Conclusion

Two important aspects in flutter investigations have been presented: First, the development of the blade deflections into global polynomials allows an accurate representation of the low-frequency eigenmodes of the blade with very few and illustrative coordinates. Second, the introduction of differential equations describing the air flow allows a very effective stability analysis.

Parameter regions of linear instability have been revealed.

References

[1] Ahrens, R., 1992, "Innere Variablen in linear-viskoelastischen Schwingungssystemen – Modellierung, numerische Behandlung und Parameteridentifikation", VDI Verlag, Düsseldorf.

[2] Antman, S.S., 1995, "Nonlinear Problems of Elasticity", *Applied Mathematical Sciences*, Springer-Verlag, New York.

[3] Blevins, R. D., 1990, Flow-Induced Vibration, 2.nd edition, Van Nostrand Reinhold, NewYork.

[4] Bremer, H., 1988, *Dynamik und Regelung Mechanischer Systeme*, Stuttgart: B.G.Teubner.

[5] Crighton, A.P., Dowling, A.P., Ffowcs Williams, J.E., Heckl, M, Leppington, F.G., 1992, "Modern Methods in Analytical Acoustics", Springer-Verlag, London.

[6] Fletcher, C.A.J., 1984, *Computational Galerkin Methods*, New York: Springer.

[7] Fuglsang, P, Antoniou, I., Bak, C., Madsen, H. A., 1998, "Wind Tunnel Test of the Risø-1 Airfoil", Risø–R–999(EN), Risø National Laboratory, Roskilde.

[8] Kant, T., Marur, S.R., Rao, G.S., 1989, *Composite Structures, Elsevier Science*, Vol.40, No.1, pp 1-9. Analytical solution to the dynamic analysis of laminated beams using higher order refined theory.

[9] Leishman, J. G., Beddows, T. S., 1986, "A Generalized Model for Airfoil Unsteady Aerodynamic Behavior and Dynamic Stall Using the Indical Method", *Proceedings, 42nd Annual Forum of the American Helicopter Society*, Washington D.C.

[10] Petersen, J.T.: A Kinematically Nonlinear Finite Element Model of a Horizontal Axis Wind Turbine. Dept. of Metrology and Wind Energy, Risø National Laboratory 1990.

[11] Spiegel, M.R., 1959, *Vector Analysis*, New York: Schaum Publishing Co.

[12] Spurk, J.H.: Strömungslehre. Berlin etc.: Springer 1996.

[13] Strang, G., 1986, *Introduction to Applied Mathematics*, Wellesley-Cambridge Press , Wellesley.

[14] Washizu, K., 1982, *Variational Methods in Elasticity and Plasticity*, 3rd edition, Oxford: Pergamon Press.

[15] Larsen, G.C., Hansen, M.H., Baumgart, A., Carlén, I., 2002, "Modal Analysis of Wind Turbine Blades", Risø–R–1181(EN), Risø National Laboratory, Roskilde.

Bibliographic Data Sheet **Risø–R–1352(EN)**

Title and author(s)

Models for Wind Turbines – a collection

Editors: Gunner C. Larsen and Morten H. Hansen
Author: Andreas Baumgart

ISBN	ISSN
87–550–3083–1 87–550–3085–8 (Internet)	0106–2840

Dept. or group	Date
Wind Energy Department	February 2002

Groups own reg. number(s)	Project/contract No.

Sponsorship	Contract No(s)
Danish Energy Authority	ENS 1363/99–0011 ENS 1363/01–0001

Pages	Tables	Illustrations	References
71	4	56	15

Abstract (Max. 2000 char.)

This report is a collection of notes which were intended to be short communications. Main target of the work presented is to supply new approaches to stability investigations of wind turbines. The author's opinion is that an efficient, systematic stability analysis can not be performed for large systems of differential equations (i.e. the order of the differential equations > 100), because numerical "effects" in the solution of the equations of motion as initial value problem, eigenvalue problem or whatsoever become predominant. It is therefore necessary to find models which are reduced to the elementary coordinates but which can still describe the physical processes under consideration with sufficiently good accuracy. Such models are presented.

Descriptors

AERODYNAMICS; BEAM MODELS; DAMPING; DYNAMIC STABILITY, FE–MODELS; HORIZONTAL AXIS TURBINES; MATHEMATICAL MODELS, STATE SPACE FORMULATION; SYSTEM IDENTIFICATION